 CMES, vol.97, no.3, pp.199-237, 2014

On the (Meshless Local Petrov-Galerkin) MLPG-Eshelby Method in Computational Finite Deformation Solid Mechanics - Part II

Z. D. Han[1] **and S. N. Atluri**[2,3]

Abstract: This paper presents a new method for the computational mechanics of large strain deformations of solids, as a fundamental departure from the currently popular finite element methods (FEM). The currently widely popular primal FEM: (1) uses element-based interpolations for displacements as the trial functions, and element-based interpolations of displacement-like quantities as the test functions; (2) uses the same type and class of trial & test functions, leading to a Galerkin approach; (3) uses the trial and test functions which are most often continuous at the inter-element boundaries; (4) leads to sparsely populated symmetric tangent stiffness matrices; (5) computes piecewise-linear predictor solutions based on the global weak-forms of the Newtonian Momentum Balance Laws for a Lagrangean Stress tensor, such as the symmetric Second Piola-Kirchhoff Stress tensor $\mathbf{S}$ [$\equiv J\mathbf{F}^{-1}\cdot\boldsymbol{\sigma}\cdot\mathbf{F}^{-t}$, where $\boldsymbol{\sigma}$ is the Cauchy Stress tensor and $\mathbf{F}$ the deformation gradient] in the initial or any other known reference configuration; and (6) computes a corrector solution, using Newton-Raphson or other Jacobian-inversion-free iterations, based on the global weak-forms of the Newtonian Momentum Balance Laws for the symmetric Cauchy Stress tensor $\boldsymbol{\sigma}$ in the current configuration. In a radical departure, the present approach blends the Energy-Conservation Laws of Noether and Eshelby, and the Meshless Local Petrov Galerkin (MLPG) Methods of Atluri, and is designated herein as the MLPG-Eshelby Method. In the MLPG-Eshelby Method, we: (1) use meshless node-based functions $\delta\mathbf{X}$, for configurational changes of the undeformed configuration, as the trial functions; (2) meshless node-based functions $\delta\mathbf{x}$, for configurational changes of the deformed configuration, as the test functions; (3) the trial functions $\delta\mathbf{X}$ and the test functions $\delta\mathbf{x}$ are necessarily different and belong to different classes of functions, thus naturally

[1] Livermore Software Technology Corporation, Livermore, CA, 94551, USA.
[2] International Collaboratory for Fundamental Studies in Engineering and the Sciences, 4131 Engineering Gateway, University of California, Irvine, Irvine, CA, 92697, USA.
[3] Fellow & Eminent Scholar, Texas Institute for Advanced Study, TAMU-3474, College Station, TX 77843, USA.

leading to a Petrov-Galerkin approach; (4) leads to sparsely populated unsymmetric tangent stiffness matrices; (5) the trial functions $\delta\mathbf{X}$, as well as the test functions $\delta\mathbf{x}$, may either be continuous or be discontinuous in their respective configurations; (6) generate piecewise-linear predictor solutions based on the local weak-forms of the Noether/Eshelby Energy Conservation Laws for the Lagrangean unsymmetric Eshelby Stress tensor $\mathbf{T}$ in the undeformed configuration [$\mathbf{T} = W\mathbf{I} - \mathbf{P}\cdot\mathbf{F}$; where $\mathbf{P} = J\mathbf{F}^{-1}\cdot\boldsymbol{\sigma}$ is the first Piola-Kirchhoff Stress tensor, and W is the stress-work density per unit initial volume of the solid] and (7) generate corrector solutions, based on Newton-Raphson or Jacobian-inversion-free iterations, using the local weak-forms of the Noether/Eshelby Energy Conservation Laws in the current configuration, for a newly introduced Eulerean symmetric Stress tensor $\tilde{\mathbf{S}}$ [which is the counter part of $\mathbf{T}$] in the current configuration [$\tilde{\mathbf{S}} = (W/J)\mathbf{I} - \boldsymbol{\sigma}$, often called by chemists as the Chemical Potential Tensor]. It is shown in the present paper that the present MLPG-Eshelby Method, based on the meshless local weak-forms of the Noether/Eshelby Energy Conservation Laws, converges much faster and leads to much better accuracies than the currently popular FEM based on the global weak-forms of the Newtonian Momentum Balance Laws. The present paper is limited to hyperelasticity, while large strains of inelastic solids will be considered in our forthcoming papers.

1 Introduction

In our earlier Part I of this paper [Han and Atluri (2014)], we have introduced the Eshelby Stress Tensor [a Lagrangean unsymmetric tensor entirely in the known undeformed configuration] $\mathbf{T} = [W\mathbf{I} - \mathbf{P}\cdot\mathbf{F}]$, where W is the strain energy density per unit undeformed volume of the finitely deformed hyperelastic anisotropic solid, $\mathbf{P}$ is the first Piola-Kirchhoff Stress tensor, and $\mathbf{F}$ is the deformation gradient. In Han and Atluri (2014) we have presented: (i) the balance laws for $\mathbf{T}$; (ii) a variety of (and an arbitrary number of) conservation laws of the Noether/Eshelby type, and the attendant "path-independent" integrals, for $\mathbf{T}$, in a defective hyperelastic anisotropic solid undergoing finite deformation and (iii) the beginning description of the (Meshless Local Petrov Galerkin) MLPG-Eshelby approach, based on the local weak-forms of the balance laws for $\mathbf{T}$, for a linear elastic solid.

In a radical departure from the currently popular finite element approaches [which are embedded in many widely used off-the-shelf software] for analyzing large strain and large rotation deformation of solids, we present in this paper an entirely different approach, which blends the energy conservation laws of Noether (1918) and Eshelby (1951,1975) and the (Meshless Local Petrov Galerkin) MLPG Methods of Atluri (1998, 2004). We designate this new approach as the MLPG-Eshelby Method for finite deformation solid mechanics. In the MLPG-Eshelby method, we:

(1) use the meshless node-based local functions $\delta\mathbf{X}$, for the configurational changes of the undeformed configuration, as the trial functions; (2) meshless node-based local functions $\delta\mathbf{x}$, for the configurational changes of the deformed configuration, as the test functions; (3) the local trial functions $\delta\mathbf{X}$ and the local test functions $\delta\mathbf{x}$ are necessarily different and belong to different classes of functions, thus naturally leading to a Local Petrov-Galerkin approach; (4) the trial function $\delta\mathbf{X}$, as well as the test function $\delta\mathbf{x}$, may either be continuous or discontinuous in their respective configurations; (5) generate piecewise-linear predictor solutions based on the local weak-forms of the Noether/Eshelby conservation laws for the Lagrangian unsymmetric Eshelby Stress tensor $\mathbf{T}$; and (6) generate corrector solutions, based on Newton-Raphson or Jacobian-inversion-free iteration, using the local weak-forms of the Noether/Eshelby conservation Laws in the current configuration, using an Eulerean symmetric stress tensor $\tilde{\mathbf{S}}$ [which is the Eulerean counterpart of $\mathbf{T}$] in the current configuration [$\tilde{\mathbf{S}} = (W/J)\mathbf{I} - \boldsymbol{\sigma}$, where $\boldsymbol{\sigma}$ is the Cauchy Stress tensor]. The present MLPG-Eshelby Method leads to sparsely populated unsymmetric tangent stiffness matrices for a finitely deforming solid.

In Section 2 of this paper, we present Newtonian momentum balance laws for $\mathbf{P}$ [the first Piola-Kirchhoff Stress tensor], $\mathbf{S}$ [the second Piola-Kirchhoff Stress tensor], and $\boldsymbol{\sigma}$ [the Cauchy Stress tensor]. We then present the Noether/Eshelby type energy conservation laws for the Lagrangean Eshelby Stress tensor $\mathbf{T}$, and their newly introduced Eulerean counterparts [$\tilde{\mathbf{S}} = (W/J)\mathbf{I} - \boldsymbol{\sigma}$; $\tilde{\boldsymbol{\tau}} = \tilde{\mathbf{S}} \cdot (\mathbf{F} \cdot \mathbf{F}^t)$], and a two-point tensor $\tilde{\mathbf{P}} = \tilde{\boldsymbol{\tau}} \cdot \mathbf{F}^{-t}$. In Section 2, we also present the tangent stiffness material coefficients, for anisotropic hyperelasticity, for use in the Newton Momentum Balance Laws and the Noether/Eshelby Energy Conservation Laws, respectively.

In Section 3, we present Meshless Local Petrov Galerkin weak-forms of the Newtonian Momentum Balance Laws, and the Noether/Eshelby Energy Conservation Laws, respectively. First, we present meshless local interpolations for the trial functions $\delta\mathbf{X}$ (configuraitonal changes of the undeformed configuration) and the test functions $\delta\mathbf{x}$ (configurational changes of the deformed configuration), respectively. We present the details of the piecewise-linear predictor solutions based on the local weak-form of the balance laws for the Lagrangean Eshelby tensor $\mathbf{T}$. We then present details of the corrector iterations using the local weak-forms of the Noether/Eshelby conservation laws, based on the Eulerean tensor $\tilde{\mathbf{S}}$. We also present a succinct summary in a Table, which shows the key differences between the popular Galerkin FEM methods, and the present MLPG-Eshelby methods, for finite deformation (large strains and large rotations) solid mechanics.

In Section 4, we present the MLPG-Eshelby methods for several linear elasto-static analyses. In Section 5, we present the numerical details of the MLPG-Eshelby methods for finite deformation analyses of a hyperelastic solid. In Section 6 we

present some conclusions.

2 Newtonian Momentum Balance Laws & Noether/Eshelby Energy Conservation Laws, Respectively, for a Variety of Stress Tensors in the Initial and Current Configurations of a Finitely Deforming Solid

2.1 Definitions of Various Stress Tensors in Initial & Current Configurations

We consider the finite deformation of a solid, wherein a material particle initially at $\mathbf{X}$, moves to a location $\mathbf{x}$. We use a fixed Cartesian coordinate system with base vectors $\mathbf{e}_i$, such that ($\mathbf{X} = X_I\mathbf{e}_i$ and $\mathbf{x} = x_i\mathbf{e}_i$). The displacement of the material particle is defined in the initial configuration, as

$$\mathbf{u}(\mathbf{X}) = \mathbf{x}(\mathbf{X}) - \mathbf{X} \quad \text{or} \quad u_i = (x_i - X_I)\mathbf{e}_i \tag{1}$$

and the *inverse displacement* from the current deformation is defined as,

$$\mathbf{v}(\mathbf{x}) = \mathbf{X}(\mathbf{x}) - \mathbf{x} = -\mathbf{u}(\mathbf{X}(\mathbf{x})) \quad \text{or} \quad v_I = (X_I - x_i)\mathbf{e}_i \tag{2}$$

Thus the deformation gradient tensor, $\mathbf{F}(\mathbf{X})$, which is a two-point tensor with the first leg in the current configuration and the second in the initial configuration, can be written as,

$$\begin{aligned} &d\mathbf{x} = \mathbf{F}\cdot d\mathbf{X} \\ &F_{iJ} = \frac{\partial x_i}{\partial X_J} \equiv x_{i,J} = u_{i,J} + \delta_{iJ} \end{aligned} \tag{3}$$

and the inverse deformation gradient tensor, $\mathbf{F}^{-1}(\mathbf{x})$, which is a two-point tensor, with the first leg in the initial configuration and the second in the current configuration, can be written as

$$\begin{aligned} &d\mathbf{X} = \mathbf{F}^{-1}\cdot d\mathbf{x} \\ &F^{-1}_{Ij} = \frac{\partial X_I}{\partial x_j} \equiv X_{I,j} = v_{I,j} + \delta_{Ij} \end{aligned} \tag{4}$$

There are infinitely many possible definitions of a stress-tensor in a finitely deformed solid, referred to both the initial and current configurations or many other intermediate configurations which involve stretches and/or rotations [see, for instance Atluri(1984)]. Among the more commonly used ones are: the Cauchy stress tensor $\boldsymbol{\sigma}$ in the current configuration; the two-point first Piola-Kirchhoff stress tensor $\mathbf{P}$ (with the first leg in the initial configuration, and the second in the current);

and the second Piola-Kirchhoff stress $\mathbf{S}$ in the initial configuration. These are related to each other, thus [see Atluri (1984)]:

$$\mathbf{P}(\mathbf{X}) = J\mathbf{F}^{-1}\cdot\boldsymbol{\sigma} = \mathbf{S}\cdot\mathbf{F}^{t} \tag{5}$$

$$\mathbf{S}(\mathbf{X}) = J\mathbf{F}^{-1}\cdot\boldsymbol{\sigma}\cdot\mathbf{F}^{-t} = \mathbf{P}\cdot\mathbf{F}^{-t} \tag{6}$$

where $J(\mathbf{X})$ is $\|\mathbf{F}(\mathbf{X})\|$, and $(\ )^t$ denotes a transpose.

One may also define the "Eshelby Stress tensor" $\mathbf{T}$ entirely in the initial configuration, [as in Han and Atluri (2014)], as:

$$\mathbf{T} = W\mathbf{I} - \mathbf{P}\cdot\mathbf{F} = W\mathbf{I} - \mathbf{S}\cdot\mathbf{C} \tag{7}$$

where $\mathbf{C} = \mathbf{F}^t\cdot\mathbf{F}$ is the right Cauchy-Green deformation tensor.

It can be shown from purely geometric considerations, that, in a finite deformation,

$$(dA\,\mathbf{N}) = \frac{1}{J}(da\,\mathbf{n})\cdot\mathbf{F} \quad \text{and} \quad (da\,\mathbf{n}) = J(dA\,\mathbf{N})\cdot\mathbf{F}^{-1} \text{ (Nansen's law)} \tag{8}$$

where $dA\,\mathbf{N}$ is an oriented differential area in the initial configuration, and $da\,\mathbf{n}$ is an oriented differential area in the current configuration.

2.2 *The material constitutive relations for use in Newtonian Momentum Balance Laws, and Noether/ Eshelby Energy Conservation Laws, Respectively & Definitions of Several Other Stress Tensors of Use in the MLPG-Eshelby Method*

Considering a general *anisotropic hyperelastic* solid, with the strain energy per unit initial volume being denoted as W, the constitutive relation for $\mathbf{P}$ may be written as [see Atluri (1984)]:

$$\mathbf{P} = \frac{\partial W}{\partial \mathbf{F}^t} \tag{9}$$

If W is a frame-indifferent function of $\mathbf{F}$ in the initial configuration, it should be a function only of $\mathbf{F}^t\cdot\mathbf{F}$. Thus [see Atluri (1984)],

$$\mathbf{P} = \frac{\partial W}{\partial \mathbf{F}^t} = \frac{\partial W}{\partial \mathbf{E}}\frac{\partial \mathbf{E}}{\partial \mathbf{F}^t} = \mathbf{S}\cdot\mathbf{F}^t \tag{10}$$

and

$$\mathbf{S} = \frac{\partial W}{\partial \mathbf{E}} = 2\frac{\partial W}{\partial \mathbf{C}} \quad \text{or} \quad S_{IJ} = \frac{\partial W}{\partial E_{IJ}} = 2\frac{\partial W}{\partial C_{IJ}} \tag{11}$$

where

$$\mathbf{E} = \frac{1}{2}(\mathbf{F}^t \cdot \mathbf{F} - \mathbf{I}) = \frac{1}{2}(\mathbf{C} - \mathbf{I}); \quad \mathbf{C} = \mathbf{F}^t \cdot \mathbf{F} = 2\mathbf{E} + \mathbf{I} \tag{12}$$

E is the Green-Lagrange Strain tensor.

Let $\tilde{W}$, the strain energy per unit *deformed configuration*, be defined in terms of the strain energy density in the initial configuration, as

$$\tilde{W}(\mathbf{x}) = W(\mathbf{X})/J \tag{13}$$

One may re-write Eq. (9) as,

$$P_{Ij} = \frac{\partial W}{\partial F_{jI}} = \frac{\partial W}{\partial F^{-1}_{Mn}} \frac{\partial F^{-1}_{Mn}}{\partial F_{jI}} = -\frac{\partial W}{\partial F^{-1}_{Mn}} F^{-1}_{Mj} F^{-1}_{In} \tag{14a}$$

or

$$\mathbf{P} = -\mathbf{F}^{-1} \cdot \frac{\partial W}{\partial \mathbf{F}^{-t}} \cdot \mathbf{F}^{-1} \tag{14b}$$

in which the following identity is used,

$$\frac{\partial F^{-1}_{Mn}}{\partial F_{jI}} = -F^{-1}_{Mj} F^{-1}_{In} \tag{15}$$

One may note that

$$\frac{\partial W}{\partial F^{-1}_{Mn}} = \frac{\partial (J\tilde{W})}{\partial F^{-1}_{Mn}} = J\frac{\partial \tilde{W}}{\partial F^{-1}_{Mn}} + \tilde{W}\frac{\partial J}{\partial F^{-1}_{Mn}} = J\frac{\partial \tilde{W}}{\partial F^{-1}_{Mn}} - \tilde{W} J F_{nM} = J\frac{\partial \tilde{W}}{\partial F^{-1}_{Mn}} - W F_{nM} \tag{16}$$

With Eq. (14), one may define,

$$\tilde{P}_{nM} \equiv \frac{\partial \tilde{W}}{\partial F^{-1}_{Mn}} = \frac{1}{J}(W F_{nM} + \frac{\partial W}{\partial F^{-1}_{Mn}}) = \frac{1}{J}(W F_{nM} - F_{nI}\frac{\partial W}{\partial F_{jI}} F_{jM}) \tag{17a}$$

or

$$\tilde{\mathbf{P}} = \frac{\partial \tilde{W}}{\partial \mathbf{F}^{-t}} = \frac{1}{J}(W\mathbf{F} - \mathbf{F} \cdot \frac{\partial W}{\partial \mathbf{F}^t} \cdot \mathbf{F}) = \frac{1}{J}(W\mathbf{F} - \mathbf{F} \cdot \mathbf{P} \cdot \mathbf{F}) = \frac{1}{J}\mathbf{F} \cdot \mathbf{T} \tag{17b}$$

which defines the constitutive relation for $\tilde{\mathbf{P}}$, which is a two-point tensor (with the first leg in the current configuration and the second in the undeformed configuration).

Comparing Eqs. (14)&(17), one may have

$$-\mathbf{F}\cdot\mathbf{P}=\tilde{\mathbf{P}}\cdot\mathbf{F}^{-1}=\frac{1}{J}(W\mathbf{I}-\mathbf{F}\cdot\mathbf{P})=\tilde{W}\mathbf{I}-\boldsymbol{\sigma}=\frac{1}{J}\mathbf{F}\cdot\mathbf{T}\cdot\mathbf{F}^{-1}\equiv\tilde{\mathbf{S}} \tag{18}$$

in which $\tilde{\mathbf{S}}$ is an Eulerean symmetric (and also called as "chemical potential tensor"), since the Cauchy stress tensor $\boldsymbol{\sigma}$ is symmetric, and it is entirely in the current configuration. With Eqs. (4) & (8), the weak-forms of the path-independent integrals for the Eshelby stress tensor may be written in terms of $\tilde{\mathbf{S}}$, in the current configuration, using the identity

$$\int_{\partial\Omega}(dA\,\mathbf{N})\cdot\mathbf{T}\cdot\delta\mathbf{X}=\int_{\partial\tilde{\Omega}}(da\,\mathbf{n})\cdot\tilde{\mathbf{S}}\cdot\delta\mathbf{x}\quad\text{for}\quad\forall\Omega \tag{19}$$

in which $\delta\mathbf{X}=\mathbf{F}^{-1}\cdot\delta\mathbf{x}$, by definition.

Let $\tilde{\mathbf{B}}$ be the left Cauchy-Green deformation tensor of the inverse deformation, defined as

$$\tilde{\mathbf{B}}=\mathbf{F}^{-1}\cdot\mathbf{F}^{-t}=\mathbf{C}^{-1} \tag{20}$$

Eq. (17) may be also rewritten as

$$\tilde{\mathbf{P}}=\frac{\partial\tilde{W}}{\partial\mathbf{F}^{-t}}=\frac{\partial\tilde{W}}{\partial\tilde{\mathbf{B}}}\frac{\partial\tilde{\mathbf{B}}}{\partial\mathbf{F}^{-t}}=2\mathbf{F}^{-1}\cdot\frac{\partial\tilde{W}}{\partial\tilde{\mathbf{B}}}\cdot\mathbf{F}^{t}\cdot\mathbf{F}^{-t}\equiv\tilde{\boldsymbol{\tau}}\cdot\mathbf{F}^{-t} \tag{21}$$

by definition, the newly-defined stress tensor $\tilde{\boldsymbol{\tau}}$ is a function of $\tilde{\mathbf{B}}$, as

$$\tilde{\boldsymbol{\tau}}=2\mathbf{F}^{-1}\cdot\frac{\partial\tilde{W}}{\partial\tilde{\mathbf{B}}}\cdot\mathbf{F}^{t}=\tilde{\mathbf{P}}\cdot\mathbf{F}^{t} \tag{22}$$

With Eqs. (18) & (21), one may have,

$$\tilde{\boldsymbol{\tau}}=\tilde{\mathbf{S}}\cdot(\mathbf{F}\cdot\mathbf{F}^{t})=\tilde{\mathbf{S}}\cdot\mathbf{B}\quad\text{or}\quad\tilde{\mathbf{S}}=\tilde{\boldsymbol{\tau}}\cdot(\mathbf{F}^{-t}\cdot\mathbf{F}^{-1}) \tag{23}$$

where $\mathbf{B}=\mathbf{F}\cdot\mathbf{F}^{t}$ is the left Cauchy-Green deformation tensor. It can be seen that the stress tensor $\tilde{\boldsymbol{\tau}}$ is not symmetric in the current configuration for a general anisotropic material. Let $j(\mathbf{x})$ be the Jacobian determinant of the inverse deformation tensor, defined as

$$j(\mathbf{x})=\left\|\mathbf{F}^{-1}(\mathbf{x})\right\|=1/J(\mathbf{X}(\mathbf{x})) \tag{24}$$

By their definitions, we may write the relations between the various stress tensors, as

$$\tilde{\mathbf{P}}=j\mathbf{F}\cdot\mathbf{T}=\tilde{\boldsymbol{\tau}}\cdot\mathbf{F}^{-t}=\tilde{\mathbf{S}}\cdot\mathbf{F} \tag{25a}$$

$$\tilde{\boldsymbol{\tau}} = J\mathbf{F}\cdot\mathbf{T}\cdot\mathbf{F}^t = \tilde{\mathbf{P}}\cdot\mathbf{F}^t = \tilde{\mathbf{S}}\cdot\mathbf{F}\cdot\mathbf{F}^t \tag{25)b}$$

$$\mathbf{T} = J\mathbf{F}^{-1}\cdot\tilde{\mathbf{P}} = J\mathbf{F}^{-1}\cdot\tilde{\boldsymbol{\tau}}\cdot\mathbf{F}^{-t} = J\mathbf{F}^{-1}\cdot\tilde{\mathbf{S}}\cdot\mathbf{F} \tag{25)c}$$

which give the duality between the stress tensors defined for forward problems $\{\mathbf{S};\mathbf{P};\boldsymbol{\sigma}\}$, and for inverse problems $\{\tilde{\boldsymbol{\tau}};\tilde{\mathbf{P}};\mathbf{T}\}$.

The stress tensors$\{\mathbf{S};\mathbf{P};\boldsymbol{\sigma}\}$ are commonly used in the Newtonian Momentum Balance Laws, while the stress tensors $\{\tilde{\boldsymbol{\tau}};\tilde{\mathbf{P}};\mathbf{T}\}$ are used in this paper to write the Noether/ Ehelby Energy Conservation Laws.

The new stress tensor $\tilde{\boldsymbol{\tau}}$ is analogous to the second Piola-Kirchhoff stress tensor $\mathbf{S}$. For isotropic materials, $\tilde{\boldsymbol{\tau}}$ becomes symmetric because $\tilde{W}$ is a function only of the right Cauchy-Green deformation tensor of the inverse deformation, $\tilde{\mathbf{C}} = \mathbf{F}^{-t}\cdot\mathbf{F}^{-1}$, as

$$\tilde{\mathbf{P}} = \frac{\partial\tilde{W}}{\partial\mathbf{F}^{-t}} = \frac{\partial\tilde{W}}{\partial\tilde{\mathbf{C}}}\frac{\partial\tilde{\mathbf{C}}}{\partial\mathbf{F}^{-t}} = 2\frac{\partial\tilde{W}}{\partial\tilde{\mathbf{C}}}\cdot\mathbf{F}^{-t} \tag{26}$$

Thus, for isotropic materials,

$$\tilde{\boldsymbol{\tau}} = 2\frac{\partial\tilde{W}}{\partial\tilde{\mathbf{C}}} \tag{27}$$

2.3 *The Newtonian Momentum Balance Laws for Finite Deformations , in terms of the stress tensors*$\{\mathbf{S};\mathbf{P};\boldsymbol{\sigma}\}$

The Newtonian equations of Linear Momentum Balance (LMB) and Angular Momentum Balance (AMB) can be written equivalently in terms of $\boldsymbol{\sigma}$, $\mathbf{P}$, and $\mathbf{S}$ [see Atluri (1984)], as:

$$\sigma_{ij,i} + \rho f_j = 0 \quad (LMB); \quad \boldsymbol{\sigma} = \boldsymbol{\sigma}^t \quad (AMB) \tag{28)a}$$

$$P_{Ij,I} + \rho_0 f_j = 0 \quad (LMB); \quad \mathbf{F}\cdot\mathbf{P} = \mathbf{P}^t\cdot\mathbf{F}^t \quad (AMB) \tag{28)b}$$

$$[S_{IK}F_{jK}]_{,I} + \rho_0 f_j = 0 \quad (LMB); \quad \mathbf{S} = \mathbf{S}^t \quad (AMB) \tag{28)c}$$

where ρ_0 is the mass density (per unit initial volume). For a homogeneous solid, ρ_0 is not a function of $\mathbf{X}$, but is a constant. As discussed in [Han and Atluri (2014)], the equivalence of Eqs. (28)a and (28)b needs to be guaranteed by the satisfaction of the geometric identity for any finite deformation, that:

$$\frac{\partial}{\partial X_I}\left(J\frac{\partial X_I}{\partial x_k}\right) = 0 \tag{29}$$

If such an equivalence is not assured in *any computational solution*, then, proper numerical corrections (iterations) need to be introduced.

2.4 The Noether/Eshelby Energy Conservation Laws for Finite Deformations of Anisotropic Solids, in terms of $\{\tilde{\boldsymbol{\tau}}; \tilde{\mathbf{P}}; \mathbf{T}\}$:

We now consider the "configuration invariance of the energy" type conservation laws arising out of Noether's (1918) Theorem. The strong form balance laws for the Eshelby Stress tensor $\mathbf{T}$, and for the stress tensors $\tilde{\mathbf{P}}$, $\tilde{\mathbf{S}}$, and $\tilde{\boldsymbol{\tau}}$ may be derived, following the procedures given in [Han and Atluri (2014)], as

$$T_{IJ,I} - \rho_0 b_J = -\left(P_{Ik,I} + \rho_0 f_k\right) F_{kJ} = 0 \tag{30a}$$

$$\tilde{P}_{iJ,i} - \rho\, b_J = 0 \tag{30b}$$

$$[JF_{Ik}^{-1}\tilde{S}_{kl}F_{lJ}]_{,I} - \rho_0\, b_J = 0 \tag{30c}$$

$$[\tilde{\tau}_{ik}F_{Jk}^{-1}]_{,i} - \rho\, b_J = 0 \tag{30d}$$

where, by definition [Han and Atluri (2014)]

$$b_J \equiv \frac{1}{\rho_0} W_{,J}\,\big|_{\text{exp.}} + f_k F_{kJ} \tag{31}$$

Again, the equivalence of Eqs. (30)a and (30)b needs to be guaranteed by the satisfaction of the geometric identity for any finite deformation, that:

$$\frac{\partial}{\partial x_i}\left(j\frac{\partial x_i}{\partial X_K}\right) = 0 \tag{32}$$

The symmetry of the Eshelby stress tensor with respect to the strain tensor $\mathbf{C}$ is mandatory, as

$$\mathbf{C}\cdot\mathbf{T} = \mathbf{T}^t\cdot\mathbf{C} \tag{33a}$$

$$\mathbf{F}^t\cdot\tilde{\mathbf{P}} = \tilde{\mathbf{P}}^t\cdot\mathbf{F} \tag{33b}$$

$$\mathbf{F}^t\cdot\tilde{\boldsymbol{\tau}}\cdot\mathbf{F}^{-t} = \mathbf{F}^{-1}\cdot\tilde{\boldsymbol{\tau}}\cdot\mathbf{F} \tag{33c}$$

$$\tilde{\mathbf{S}} = \tilde{\mathbf{S}}^t \tag{33d}$$

2.5 The Tangential Material Stiffness Coefficients for Anisotropic Hyperelasticity, for use in Piecewise Linear Weak Forms of the Newtonian Momentum Balance & Noether/ Eshelby Energy Conservation Laws, Respectively:

We now consider the "incremental" variables, as may be suitable for computational analyses of quasi-static finite deformations of solids. Let $\Delta\mathbf{u}$ be the incremental

displacement of a material particle from the current configuration, $C^{(N)}$, to the next configuration $C^{(N+1)}$. To this end, we define incremental variables in $C^{(N)}$,

$$\Delta\mathbf{L} = \frac{\partial \Delta\mathbf{u}}{\partial \mathbf{x}} = \Delta\mathbf{D} + \Delta\mathbf{W} \quad \text{or} \quad \Delta L_{ij} = \frac{\partial \Delta u_i}{\partial x_j} = \Delta D_{ij} + \Delta W_{ij} \tag{34a}$$

$$\Delta\mathbf{D} = \frac{1}{2}(\Delta\mathbf{L} + \Delta\mathbf{L}^t) \quad \text{or} \quad \Delta D_{ij} = \frac{1}{2}(\Delta L_{ij} + \Delta L_{ji}) \tag{34b}$$

$$\Delta\mathbf{W} = \frac{1}{2}(\Delta\mathbf{L} - \Delta\mathbf{L}^t) \quad \text{or} \quad \Delta W_{ij} = \frac{1}{2}(\Delta L_{ij} - \Delta L_{ji}) \tag{34c}$$

The incremental deformation gradient tensor can be computed, by definition, as

$$\Delta F_{iJ} = \frac{\partial \Delta u_i}{\partial X_J} = \frac{\partial \Delta u_i}{\partial x_j} F_{jJ} = \Delta L_{ij} F_{jJ} \quad \text{and} \quad \Delta L_{ij} = \Delta F_{iJ} F^{-1}_{Jj} \tag{35}$$

$$\Delta E_{KL} = \frac{1}{2}(F_{kK}\Delta L_{lk} F_{lL} + F_{kK}\Delta L_{kl} F_{lL}) = F_{kK}\Delta D_{kl} F_{lL} \tag{36}$$

Thus, for a general anisotropic hyperelastic solid, the constitutive relation in Eq. (11) gives the stress increment in the undeformed configuration, $C^{(0)}$, as:

$$\Delta S_{IJ} = \frac{\partial^2 W}{\partial E_{IJ}\partial E_{KL}} F_{kK}\Delta D_{kl} F_{lL} = \frac{\partial^2 W}{\partial E_{IJ}\partial E_{KL}} F_{kK} F_{lL}\Delta D_{kl} \tag{37}$$

which defines the forth-order tangential material stiffness tensor. Eq. (37) is often used in the piecewise linear weak forms of the Newtonian Momentum Balance Laws.

To apply the Noether/ Eshelby energy conservation laws, we first let $\tilde{\mathbf{v}}(\mathbf{X})$ be the configurational changes in the undeformed configuration of the solid, $C^{(0)}$, and we define the incremental displacements in the current configuration, $C^{(N)}$, induced due to $\tilde{\mathbf{v}}(\mathbf{X})$, be written as,

$$\Delta\mathbf{u} = \mathbf{F}\cdot\tilde{\mathbf{v}} \quad \text{or} \quad \Delta u_i = F_{iJ}\tilde{v}_J \tag{38}$$

We note that:

$$\Delta L_{ij} = \frac{\partial \Delta u_i}{\partial x_j} = F_{iK}\frac{\partial \tilde{v}_K}{\partial x_j} = F_{iK}\frac{\partial \tilde{v}_K}{\partial X_L} F^{-1}_{Lj} \equiv F_{iK} F^{-1}_{Lj}\Delta L^*_{KL} \quad \text{or} \quad \Delta\mathbf{L} = \mathbf{F}\cdot\Delta\mathbf{L}^*\cdot\mathbf{F}^{-1} \tag{39a}$$

and, with Eq. (34)b,

$$\Delta D_{ij} = \frac{1}{2}[F_{iK}F^{-1}_{Lj}\Delta L^*_{KL} + F^{-1}_{Li}F_{jK}\Delta L^*_{KL}] = \frac{1}{2}[F_{iK}F^{-1}_{Lj} + F^{-1}_{Li}F_{jK}]\Delta L^*_{KL} \tag{39b}$$

in which, by definition, $\Delta\mathbf{L}^*$ is the gradient of $\tilde{\mathbf{v}}(\mathbf{X})$ as

$$\Delta\mathbf{L}^* = \frac{\partial\Delta\tilde{\mathbf{v}}}{\partial\mathbf{X}} \quad \text{or} \quad \Delta L^*_{KL} = \frac{\partial\tilde{v}_K}{\partial X_L} \tag{40}$$

Substituting Eq. (39)b into Eq. (37), the tangential material stiffness relations, for use in the piecewise linear weak forms of the Noether/Eshelby energy conservation laws, may be written as,

$$\Delta S_{IJ} = \frac{1}{2}\frac{\partial^2 W}{\partial E_{IJ}\partial E_{MN}} F_{kM}F_{lN}[F_{kK}F^{-1}_{Ll} + F^{-1}_{Lk}F_{lK}]\Delta L^*_{KL} \equiv C^*_{IJKL}\Delta L^*_{KL} \tag{41}$$

Eq. (41) are the incremental constitutive laws, in the context of the present Energy-Conservation Laws of Noether and Eshelby, wherein the configurational changes $\tilde{\mathbf{v}}(\mathbf{X})$, and the corresponding gradients $\Delta\mathbf{L}^*$ are considered. $\Delta\mathbf{S}$ and $\Delta\mathbf{L}^*$ may be considered as a conjugate pair in postulating a piecewise linear constitutive relation in the present context of the Noether/Eshelby energy conservation laws. On other hand, the material constitutive laws may be postulated in the current configuration in terms of Jaumann rate of the Kirchhoff stress $\boldsymbol{\sigma}^* = (J\boldsymbol{\sigma})$, or any of the infinitely many other objective stress-rates, for either hyperelastic or hypoelastic materials Atluri (1975, 1980, 1982, 1983, 1984). The corresponding constitutive relation for use in the Noether/Eshelby energy conservation laws is formulated in terms of $\Delta\mathbf{L}^*$ in Appendix A.

3 Meshless Local MLPG (Meshless Local Petrov-Galerkin) Weak-forms of the Newtonian Momentum Balance Laws & the Noether/Eshelby Energy Conservation Laws, Respectively:

3.1 Meshless interpolations of trial and test functions: Various Primal & Mixed MLPG-Eshelby Methods:

As mentioned earlier, the local trial functions in the presently proposed MLPG-Eshelby method are $\delta\mathbf{X}$, the configurational changes in the undeformed configuration; and the local test functions are $\delta\mathbf{x}$, the configurational changes in the deformed configuration. Below, we give the details of these local trial and test functions, based on the Meshless Local Petrov Galerkin (MLPG) approach developed by Atluri (1998, 2004).

Among the many meshless approximation schemes, the moving least squares (MLS) is generally considered to be one of the best methods to interpolate random data with a reasonable accuracy, because of its locality, completeness, robustness and continuity. The MLS has been widely used in constructing trial functions in many types of MLPG meshless methods [Atluri (2004)], and also for the test

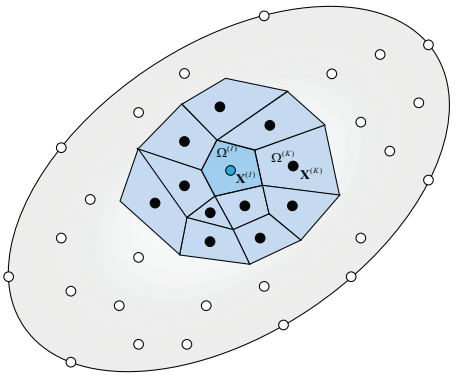

Figure 1: A meshless local interpolation in a local sub-domain near node I at point $\mathbf{X}^{(I)} \in \Omega^{(I)}$ in the undeformed configuration

functions in the Galerkin methods. Various MLPG methods however employ may different types of test functions [Atluri (2004)]. In the present paper, the MLS approximation is used to construct the trial functions $\tilde{\mathbf{v}}(\mathbf{X})$ based on the fictitious nodal value $\hat{\mathbf{v}}^{(K)}$ [Atluri (2004)], as

$$\begin{aligned} &\tilde{\mathbf{v}}^{MLS}(\mathbf{X}) = \sum_{K=1}^{n} \Phi^{(K)}(\mathbf{X})\hat{\mathbf{v}}^{(K)} \\ &\Delta\mathbf{L}^{*MLS}(\mathbf{X}) = \frac{\partial \tilde{\mathbf{v}}^{MLS}}{\partial \mathbf{X}}(\mathbf{X}) \end{aligned} \qquad \text{for} \quad \forall \mathbf{X} \in \Omega^{(I)} \tag{42}$$

where the gradients $\Delta\mathbf{L}^{*}(\mathbf{X})$ are derived from $\tilde{\mathbf{v}}(\mathbf{X})$ through direct differentiation. The continuity of the trial functions $\tilde{\mathbf{v}}^{MLS}$ is dependent on that of the weight functions $w^{(K)}$ in the MLS interpolation [Atluri (2004)]. In the present study, we choose the fourth-order spline function as the weight function, which leads to a continuous trial function in the local domain.

Secondly, a mixed-type of interpolation may also be used for constructing the trial functions $\tilde{\mathbf{v}}(\mathbf{X})$ and their gradients $\Delta\mathbf{L}^{*}(\mathbf{X})$ based on the fictitious nodal value $\hat{\mathbf{v}}^{(K)}$ [Atluri, Han and Rajendran (2004)] over each local sub-domain, as

$$\begin{aligned} &\Delta\mathbf{L}^{*(I)} \equiv \Delta\mathbf{L}^{*MLS}(\mathbf{X}^{(I)}) = \frac{\partial \tilde{\mathbf{v}}^{MLS}}{\partial \mathbf{X}}(\mathbf{X}^{(I)}) \\ &\Delta\mathbf{L}^{*MIX}(\mathbf{X}) = \sum_{K=1}^{n} \Psi^{(K)}(\mathbf{X})\Delta\mathbf{L}^{*(K)} \\ &\tilde{\mathbf{v}}^{MIX}(\mathbf{X}) = \tilde{\mathbf{v}}^{MIX}\left(\Delta\mathbf{L}^{*MIX}(\mathbf{X}), \mathbf{X}\right) \end{aligned} \qquad \text{for} \quad \forall \mathbf{X} \in \Omega^{(I)} \tag{43}$$

In the interpolation for $\Delta\mathbf{L}^*(\mathbf{X})$ in Eq. (43), $\Psi^{(K)}$ are independent from the interpolation for $\tilde{\mathbf{v}}(\mathbf{X})$ in Eq. (42), $\Phi^{(K)}$. In the present study, $\Delta\mathbf{L}^*(\mathbf{X})$ is assumed to be constant within each sub-domain, as

$$\begin{aligned} &\Delta\mathbf{L}^{*MIX}(\mathbf{X}) = \Delta\mathbf{L}^{*(I)} \\ &\tilde{\mathbf{v}}^{MIX}(\mathbf{X}) = \Delta\mathbf{L}^{*MIX} \cdot \left(\mathbf{X} - \mathbf{X}^{(I)}\right) \end{aligned} \quad \text{for} \quad \forall \mathbf{X} \in \Omega^{(I)} \tag{44}$$

It is clear that the trial functions $\tilde{\mathbf{v}}^{MIX}(\mathbf{X})$ and $\Delta\mathbf{L}^{*MIX}(\mathbf{X})$ are piece-wise continuous, but are discontinuous at the boundaries of each local sub-domain $\partial\Omega^{(I)}$. It also implies that the local sub-domains need to be non-overlapping in the global solution domain, as shown in Fig. 1. Thus, the trial functions become unique for each unique material point $\mathbf{X}$, except for the discontinuities at the boundaries between the non-overlapping local sub-domains. In the present study, a non-overlapping partition of the global domain is constructed with the use of the Delaunay tessellation of a given set of nodes for 2D or 3D problems. The quality of the virtual-mesh of 2D Delaunay triangulation and 3D Delaunay tetrahedralization is not important, as the virtual-mesh is simply used to partition the solution domain, instead of using such a virtual-mesh for interpolating the solution variables as is done in many mesh-based FEM. Each triangle may be sub-divided into three parts by three segments connecting its centroid to the middle points of the sides of the triangle, as shown in Fig. 2. A local sub-domain for a node is created by merging the parts of all its neighboring triangles, as a non-convex partition. Each tetrahedron may also be partitioned for 3D problems accordingly.

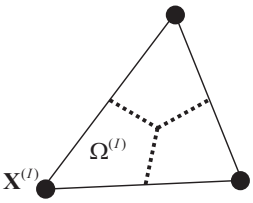

Figure 2: A partition of a triangle.

In the present study, the mixed-type interpolation is also applied to the stress variables, such as $\boldsymbol{\sigma}(\boldsymbol{\varsigma})$, based on the corresponding nodal values computed in Eq. (42). The linear shape functions $N^{(M)}(\boldsymbol{\varsigma})$ for 2D triangles or 3D tetrahedrons may be adopted to interpolate the stress variables, by replacing $\Psi^{(K)}$ in Eq. (43), as,

$$\boldsymbol{\sigma}^{MIX}(\boldsymbol{\varsigma}) = \sum_{M} N^{(M)}(\boldsymbol{\varsigma})\,\boldsymbol{\sigma}^{(M)} \tag{45}$$

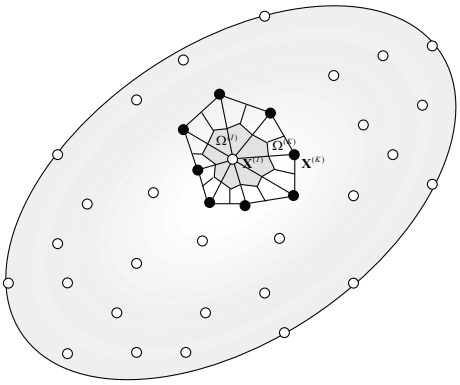

Figure 3: A non-overlapping local sub-domain (the darkly shaded polygon) defined for node I based on the Delaunay tessellation.

Thus, the trial functions for stresses are continuous and piece-wise flat, without any gaps. The corresponding domain integrals become constant during finite deformation, resulting in a constant global matrix transferring the corresponding stress variables into the internal forces.

In general, the MLS shape function does not have the Dirac Delta property. Many other approximation methods are also available for evaluating the nodal coefficients based on the true nodal coordinates, including the compact radius basis function (cRBF) methods. A revised MLS interpolation possessing the Dirac Delta property will be also proposed in our forthcoming papers for explicit dynamic problems, for computational efficiency.

3.2 The Meshless Test Functions

In the MLPG Eshelby methods, the test functions are the configurational changes of the deformed configuration. They can be chosen independently, to make it more suitable for the numerical implementation. In the present study, we define two types of these test functions. In the first method, Heaviside functions are chosen to be the test functions within each local test sub-domain, as

$$\delta \mathbf{x}^{FVM}(\mathbf{X}) = \delta \mathbf{x}^{(I)} = constant \quad \text{for} \quad \forall \mathbf{X} \in \Omega^{(I)} \tag{46}$$

in which $\delta \mathbf{x}^{(I)}$ are the variations of the vertex nodes. These test functions correspond to the imaginary operations of "cutting stresses" in [Eshelby (1975)]. The constant test functions make the MLPG Eshelby methods computationally very efficient, because all domain integrals vanish for piece-wise linear materials. When

Heaviside test functions are used, we call the resultant methods as the Finite Volume MLPG-Eshelby Methods

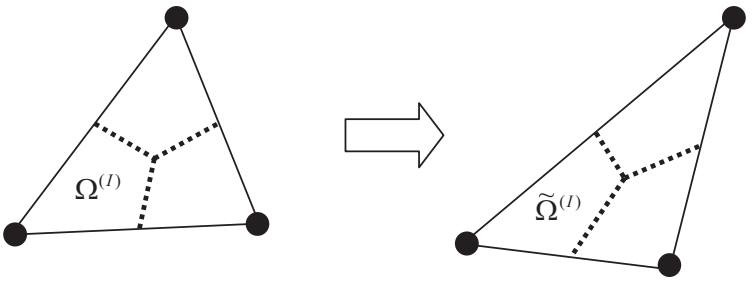

Figure 4: A partition of a triangle.

Alternatively linear shape functions for 2D triangles or 3D tetrahedrons may be adopted to be the test functions within triangles or tetrahedrons, as

$$\delta \mathbf{x}^{FEM}(\boldsymbol{\varsigma}) = \sum_{M} N^{(M)}(\boldsymbol{\varsigma})\, \delta \mathbf{x}^{(M)} \tag{47}$$

We call the resultant methods as Linear Test Function MLPG-Eshelby Methods.

3.3 Local Weakforms of the Newtonian Momentum Balance Laws in the Meshless MLPG Method

It is well known that the Newtonian momentum balance laws for the Cauchy stress tensor in Eq. (28)a are not convenient for writing the weakforms in the initial configuration. It is more convenient to write the Newtonian Momentum Balance Laws of the first or the second Piola-Kirchhoff stress tensors as in Eq. (28)b in the initial configuration.

Let $\mathbf{u}(\mathbf{X})$ be the trial functions for displacements, and we satisfy Eq. (9) in terms of $\mathbf{F}(\mathbf{X})$. Let $\delta\mathbf{u}(\mathbf{X})$ be the test functions which are used to satisfy the momentum balance laws of $\mathbf{P}$ in Eq. (28)b in a weak form for a finitely deformed solid. Many MLPG weakforms can be written within any local sub-domain $\Omega^{(I)}$ in a solid Ω, i.e. $\Omega^{(I)} \subset \Omega$, through the Meshless Local Petrov Galerkin approach [Atluri (2004)].

A local *scalar* weak form of Eq. (28)c can then be written in the initial configuration for each sub-domain, as,

$$\int_{\Omega^{(I)}} (S_{IM} F_{j,M})_{,I} \delta u_j d\Omega + \int_{\Omega^{(I)}} \rho_0 f_j \delta u_j d\Omega = 0 \tag{48}a$$

or

$$\int_{\partial\Omega^{(I)}} N_I (S_{IM} F_{j,M}) \delta u_j dS - \int_{\Omega^{(I)}} (S_{IM} F_{j,M}) \delta u_{j,I} d\Omega + \int_{\Omega^{(I)}} \rho_0 f_j \delta u_j d\Omega = 0 \qquad (48)\text{b}$$

We may also write a local *vector* weak form of Eq. (28)c by using the gradients of the test functions, $\delta u_{i,L}$, if the geometric identity in Eq. (28)d is not satisfied [Han and Atluri (2003)], as :

$$\int_{\Omega^{(I)}} (S_{IM} F_{j,M})_{,I} \delta u_{j,L} d\Omega + \int_{\Omega^{(I)}} \rho_0 f_j \delta u_{j,K} d\Omega = 0 \qquad (49)\text{a}$$

or

$$\int_{\partial\Omega^{(I)}} e_{ILk} (S_{IM} F_{j,M}) D_k \delta u_j dS - \int_{\Omega^{(I)}} (S_{IM} F_{j,M})_{,L} \delta u_{j,I} d\Omega + \int_{\Omega^{(I)}} \rho_0 f_j \delta u_{j,L} d\Omega = 0 \qquad (49)\text{b}$$

where the surface tangential operator D_t is defined as,

$$D_t = N_R \, e_{RSt} \frac{\partial}{\partial X_S} \qquad (50)$$

With the various local weakforms in Eqs. (48) & (49), and various choices of local trial and test functions as described in the previous Section, the MLPG approach provides many choices in developing Primal, and Mixed MLPG methods, as has been well documented in [Atluri (2004)].

3.4 Local Weakforms of the Noether/ Eshelby Energy Conservation Laws for Various MLPG-Eshelby Methods, for Generating Picewise-Linear Predictor Solutions for Finite Deformations:

The Eshelby stress tensor **T** is defined in the initial configuration, and it is a nonlinear function of **F** even for small-strain linear elastic material behavior. The local weakforms of the energy conservation laws in Eq. (30) are now written for finite deformations, and are linearized using the tangential material stiffness in its incremental form, to develop piece-wise linear predictor solutions, based on the MLPG-Eshelby methods.

We refer the solution variables (displacements, deformation gradient, and stresses) in the state $C^{(N+1)}$ to the configuration of the body in the immediately preceding state, denoted as $C^{(N)}$, which is presumed to be known, including the variables in $C^{(N)}$, such as **u**, **F**, $\boldsymbol{\sigma}$ and **T**, with the initial configuration $C^{(0)}$ being the reference configuration, as shown in Fig. 5. The solution variables in the preceding state $C^{(N)}$ may also be the Mth trial solution during the iteration process, which may not

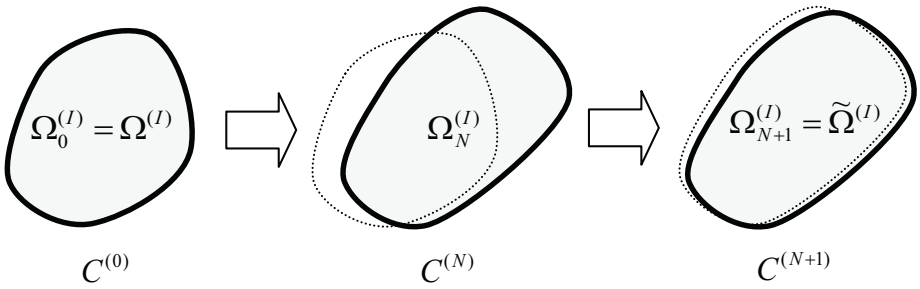

Figure 5: Three configurations during a finite deformation.

satisfy the balance laws. Let $\mathbf{X}$ and $\mathbf{x}$ be the Cartesian spatial coordinates of a particle in the initial configuration c and the deformed configuration $C^{(N)}$, respectively. Let $\tilde{\mathbf{v}}(\mathbf{X})$ be the configurational changes of the initial configuration which are the trial functions in the present MLPG-Eshelby approach, and let the corresponding changes to the displacements in $C^{(N)}$ as given in Eq. (38), be $\Delta\mathbf{u}(\mathbf{X})$. We now solve for the corresponding stress increments from $C^{(N)}$ to $C^{(N+1)}$. By first taking $\delta\mathbf{X}$ as the test functions, one may write the MLPG-Eshelby local weakforms of the energy conservation laws in Eq. (30)a for each local sub-domain $\Omega^{(I)}$ in the initial configuration $C^{(0)}$, for the variables in the deformed configuration $C^{(N+1)}$, as,

$$\int_{\Omega^{(I)}} T_{IJ,I}^{(N+1)} \delta X_J d\Omega = \int_{\Omega^{(I)}} \rho_0 b_J^{(N+1)} \delta X_J d\Omega \tag{51a}$$

If all trial solution variables are continuous within each local sub-domain $\Omega^{(I)}$, an alternate weakform may be written for each local sub-domain, from Eq. (30)b, as,

$$\int_{\Omega^{(I)}} P_{Ij,I}^{(N+1)} F_{jK}^{(N+1)} \delta X_K d\Omega + \int_{\Omega^{(I)}} \rho_0 f_j^{(N+1)} F_{jK}^{(N+1)} \delta X_K d\Omega = 0 \tag{51b}$$

As the test functions may be assumed independently, one may replace $\delta\mathbf{X}$ with some other test functions, denoted as $\delta\mathbf{x}$, within each sub-domain $\Omega^{(I)}$, in which $\mathbf{F}^{(N+1)}$ are continuous, as

$$\delta x_j = F_{jK}^{(N+1)} \delta X_K \tag{52}$$

Thus the weakform in Eq. (51)b may be re-written as,

$$\int_{\Omega^{(I)}} P_{Ij,I}^{(N+1)} \delta x_j d\Omega + \int_{\Omega^{(I)}} \rho_0 f_j^{(N+1)} \delta x_j d\Omega = 0 \tag{51c}$$

With Eq. (5), the above weakform may be also written in terms of the Cauchy stress in the configuration $C^{(N+1)}$, as

$$\int_{\Omega_{N+1}^{(I)}} \sigma_{ij,i}^{(N+1)} \delta x_j d\Omega + \int_{\Omega_{N+1}^{(I)}} \rho f_j^{(N+1)} \delta x_j d\Omega = 0 \tag{51d}$$

As the configuration $C^{(N+1)}$ is yet unknown, the solution variables may be linearized from their values in the immediately preceding state [i.e. the configuration $C^{(N)}$], as

$$\int_{\Omega_N^{(I)}} \left[\left(S_{(N)}^{(N+1)} \right)_{IJ} \left(F_{(N)}^{(N+1)} \right)_{jJ} \right]_{,I} \delta x_j d\Omega + \int_{\Omega_N^{(I)}} \rho_N \left[f_j^{(N)} + \Delta f_j \right] \delta x_j d\Omega = 0 \quad (51)\text{e}$$

where $\left(\bullet_{(N)}^{(N+1)} \right)$ denotes a variable in configuration $C^{(N+1)}$ with the configuration $C^{(N)}$ as the reference configuration.

The first integrand in Eq. (51)e may be linearized in the incremental forms, as

$$\begin{aligned} &\left[\left(S_{(N)}^{(N+1)} \right)_{IJ} \left(F_{(N)}^{(N+1)} \right)_{jJ} \right]_{,I} = \left[\left(\sigma_{IJ}^{(N)} + \left(\Delta S_{(N)}^{(N+1)} \right)_{IJ} \right) \left(\delta_{jJ} + \left(\Delta F_{(N)}^{(N+1)} \right)_{jJ} \right) \right]_{,I} \\ &= \left[\sigma_{IJ}^{(N)} + \left(\Delta S_{(N)}^{(N+1)} \right)_{IJ} + \sigma_{IJ}^{(N)} \left(\Delta F_{(N)}^{(N+1)} \right)_{jJ} \right]_{,I} \end{aligned} \quad (53)$$

One may notice that

$$\begin{aligned} \boldsymbol{\sigma}^{(N+1)} &= \frac{1}{J^{(N+1)}} \left(\mathbf{F}_{(0)}^{(N+1)} \right) \cdot \left(\mathbf{S}_{(0)}^{(N+1)} \right) \cdot \left(\mathbf{F}_{(0)}^{(N+1)} \right)^t \\ &= \frac{J^{(N)}}{J^{(N+1)}} \left(\mathbf{F}_{(N)}^{(N+1)} \right) \cdot \left(\mathbf{S}_{(N)}^{(N+1)} \right) \cdot \left(\mathbf{F}_{(N)}^{(N+1)} \right)^t \end{aligned} \quad (54)$$

Thus,

$$\left(\mathbf{S}_{(N)}^{(N+1)} \right) = \frac{1}{J^{(N)}} \left(\mathbf{F}_{(0)}^{(N)} \right) \cdot \left(\mathbf{S}_{(0)}^{(N+1)} \right) \cdot \left(\mathbf{F}_{(0)}^{(N)} \right)^t \quad (55)$$

By definition, one may have

$$\begin{aligned} \mathbf{S}_{(N)}^{(N+1)} &= \boldsymbol{\sigma}^{(N)} + \Delta \mathbf{S}_{(N)}^{(N+1)} \\ \mathbf{S}_{(0)}^{(N+1)} &= \mathbf{S}_{(0)}^{(N)} + \Delta \mathbf{S}_{(0)} \\ \boldsymbol{\sigma}^{(N)} &= \frac{1}{J^{(N)}} \left(\mathbf{F}_{(0)}^{(N)} \right) \cdot \left(\mathbf{S}_{(0)}^{(N)} \right) \cdot \left(\mathbf{F}_{(0)}^{(N)} \right)^t \end{aligned} \quad (56)$$

Substituting Eq. (56) into Eq. (55), the tangential material stiffness for $\Delta \mathbf{S}_{(N)}^{(N+1)}$ can be written as,

$$\Delta \mathbf{S}_{(N)}^{(N+1)} = \frac{1}{J^{(N)}} \left(\mathbf{F}_{(0)}^{(N)} \right) \cdot \left(\Delta \mathbf{S}_{(0)} \right) \cdot \left(\mathbf{F}_{(0)}^{(N)} \right)^t \quad (57)$$

With the tangential material stiffness for $\Delta\mathbf{S}_{(0)}$ in the initial configuration as in Eq. (41), one may have the spatial tangential material stiffness for $\Delta\mathbf{S}^{(N+1)}_{(N)}$ in the configuration $C^{(N)}$, as

$$\left(\Delta S^{(N+1)}_{(N)}\right)_{ij} = \frac{1}{J^{(N)}}\left(F^{(N)}_{(0)}\right)_{iM}\cdot\left(C^{*}_{MNKL}\Delta L^{*}_{KL}\right)\cdot\left(F^{(N)}_{(0)}\right)_{jN} \equiv c^{*}_{ijKL}\Delta L^{*}_{KL} \tag{58}$$

With Eqs. (58) & (39)a, the incremental stress in Eq. (53) can be linearized with respect to $\Delta\mathbf{L}^{*}$ as,

$$\left(\Delta S^{(N+1)}_{(N)}\right)_{IJ} + \sigma^{(N)}_{IM}\left(\Delta F^{(N+1)}_{(N)}\right)_{jM} = c^{*}_{ijKL}\Delta L^{*}_{KL} + \sigma^{(N)}_{IM}F_{jK}F^{-1}_{LM}\Delta L^{*}_{KL} \equiv c^{tangent}_{ijKL}\Delta L^{*}_{KL} \tag{59}$$

Substituting Eqs. (59)&(53) into Eq. (51)e, one may have the local weakforms of the energy conservation laws, by applying the divergence theorem to the first integrand in Eq. (51)e, as,

$$\begin{aligned}&\int_{\partial\Omega^{(I)}_{N}} n_i\left[\sigma^{(N)}_{ij} + c^{tangent}_{ijKL}\Delta L^{*}_{KL}\right]\delta x_j dS - \int_{\Omega^{(I)}_{N}}\left[\sigma^{(N)}_{ij} + c^{tangent}_{ijKL}\Delta L^{*}_{KL}\right]\delta x_{j,i}d\Omega \\ &+ \int_{\Omega^{(I)}_{N}}\rho_N\left[f^{(N)}_{j} + \Delta f_j\right]\delta x_j d\Omega = 0\end{aligned} \tag{60}$$

or

$$\begin{aligned}&\left\{\int_{\partial\Omega^{(I)}_{N}} n_i c^{tangent}_{ijKL}\Delta L^{*}_{KL}\delta x_j dS - \int_{\Omega^{(I)}_{N}} c^{tangent}_{ijKL}\Delta L^{*}_{KL}\delta x_{j,i}d\Omega\right\} + \left\{\int_{\Omega^{(I)}_{N}}\rho_N\Delta f_j\delta x_j d\Omega\right\} \\ &+ \left\{\int_{\partial\Omega^{(I)}_{N}} n_i\sigma^{(N)}_{ij}\delta x_j dS - \int_{\Omega^{(I)}_{N}}\sigma^{(N)}_{ij}\delta x_{j,i}d\Omega + \int_{\Omega^{(I)}_{N}}\rho_N f^{(N)}_{j}\delta x_j d\Omega\right\} = 0\end{aligned} \tag{61}a$$

in which the first term corresponds to the tangential stiffness matrix of the local solid domain; the second term to the load increments; and the last term to the residual forces. All variables are defined in the configuration $C^{(N)}$ within a local sub-domain.

If the configurational changes $\tilde{\mathbf{v}}$ (meshless local trial functions) in the intial configuration, and the configurational changes $\delta\mathbf{x}$ (meshless local test functions) in the current configuration, are both continuous between the non-overlapping sub-domains, Eq. (61)a is equivalent to the weakform of the Eshelby stress tensor in Eq. (51)a if the geometric identity is satisfied. However, it is very hard to construct the trial functions $\tilde{\mathbf{v}}$, as well as the corresponding displacement variation $\Delta\mathbf{u}$, to

be continuous and satisfy the geometric identity globally. In the present study, the trial functions $\tilde{\mathbf{v}}$ are constructed to be continuous and satisfy the geometric identify within each local sub-domain only, and are allowed be discontinuous between the non-overlapping sub-domains. One may introduce an additional term in the integral over the boundaries of the non-overlapping subdomains, of Eq. (51)a into Eq. (61)a, by assuming that any variable $\mathbf{A}(\zeta)$ is linear across the inter-subdomain boundary between local non-overlapping subdomains, along the direction normal to the boundary, as,

$$\mathbf{A}(\zeta) = (1-\zeta)\,\mathbf{A}^{(I)} + \zeta\,\mathbf{A}^{(J)} \tag{62}$$

where $\partial\Omega^{(IJ)}$ is the boundary-segment between the non-overlapping local subdomains $\Omega^{(I)}$ and $\Omega^{(J)}$ with the parameter ζ being as shown in Fig. 6.

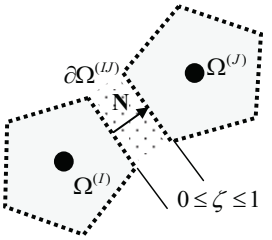

Figure 6: A shared boundary between two local sub-domains.

One may write this additional term separately for the preceding solution $\mathbf{u}(\mathbf{X})$ and the solution $\tilde{\mathbf{v}}(\mathbf{X})$ for the configurational changes in the initial configuration, in a similar manner, as

$$\begin{aligned}
&\left\{ \int_{\partial\Omega_N^{(IJ)}} n_i \left[\left(c_{ijKL}^{tangent} \Delta L_{KL}^{*} \delta x_j \right)^{(J)} - \left(c_{ijKL}^{tangent} \Delta L_{KL}^{*} \delta x_j \right)^{(I)} \right] dS \right. \\
&- \frac{1}{2} \int_{\partial\Omega_N^{(IJ)}} \left[\left(c_{ijKL}^{tangent} \Delta L_{KL}^{*} \right)^{(J)} + \left(c_{ijKL}^{tangent} \Delta L_{KL}^{*} \right)^{(I)} \right] \left(\delta x_j^{(J)} - \delta x_j^{(I)} \right) dS \Big\} \\
&+ \left\{ \int_{\partial\Omega_N^{(IJ)}} n_i \left[\left(\sigma_{ij}^{(N)} \delta x_j \right)^{(J)} - \left(\sigma_{ij}^{(N)} \delta x_j \right)^{(I)} \right] dS \right. \\
&\left. - \frac{1}{2} \int_{\partial\Omega_N^{(IJ)}} \left[\left(\sigma_{ij}^{(N)} \right)^{(J)} + \left(\sigma_{ij}^{(N)} \right)^{(I)} \right] \left(\delta x_j^{(J)} - \delta x_j^{(I)} \right) dS \right\}
\end{aligned} \tag{63}$$

which needs to be added into Eq. (61)a to form the global stiffness equations if discontinuous trial and test functions are used. Thus the local weakforms of the

energy conservation laws can be written as,

$$\left\{\int_{\Omega_N^{(I)}} c_{ijKL}^{tangent}\Delta L_{KL}^{*}\delta x_{j,i}d\Omega+\int_{\partial\Omega_N^{(IJ)}}\frac{1}{2}\left[\left(c_{ijKL}^{tangent}\Delta L_{KL}^{*}\right)^{(J)}+\left(c_{ijKL}^{tangent}\Delta L_{KL}^{*}\right)^{(I)}\right]\left(\delta x_j^{(J)}-\delta x_j^{(I)}\right)dS\right\}$$
$$=\left\{\int_{\Omega_N^{(I)}}\rho_N\Delta f_j\delta x_j d\Omega\right\}$$
$$+\left\{\int_{\Omega_N^{(I)}}\rho_N f_j^{(N)}\delta x_j d\Omega-\int_{\Omega_N^{(I)}}\sigma_{ij}^{(N)}\delta x_{j,i}d\Omega-\int_{\partial\Omega_N^{(IJ)}}\frac{1}{2}\left[\left(\sigma_{ij}^{(N)}\right)^{(J)}+\left(\sigma_{ij}^{(N)}\right)^{(I)}\right]\left(\delta x_j^{(J)}-\delta x_j^{(I)}\right)dS\right\} \tag{61)b}$$

With a constant test function $\delta\mathbf{x}$ over each local sub-domain, the domain integrals vanish and the local weak forms of the energy conservation laws may be further simplified as,

$$\left\{\int_{\partial\Omega_N^{(IJ)}}\frac{1}{2}\left[\left(c_{ijKL}^{tangent}\Delta L_{KL}^{*}\right)^{(J)}+\left(c_{ijKL}^{tangent}\Delta L_{KL}^{*}\right)^{(I)}\right]\left(\delta x_j^{(J)}-\delta x_j^{(I)}\right)dS\right\}$$
$$=\left\{\int_{\Omega_N^{(I)}}\rho_N\Delta f_j\delta x_j d\Omega\right\}$$
$$+\left\{\int_{\Omega_N^{(I)}}\rho_N f_j^{(N)}\delta x_j d\Omega-\int_{\partial\Omega_N^{(IJ)}}\frac{1}{2}\left[\left(\sigma_{ij}^{(N)}\right)^{(J)}+\left(\sigma_{ij}^{(N)}\right)^{(I)}\right]\left(\delta x_j^{(J)}-\delta x_j^{(I)}\right)dS\right\} \tag{61)c}$$

This method is computationally extremely efficient, since: i) no domain integrals are involved except when the body forces exist; ii) all derivatives are evaluated at nodal points only; iii) one point integral per one shared boundary segment may be used.

Once the trial functions $\tilde{\mathbf{v}}(\mathbf{X})$ (configurational changes in the initial configuration) are solved through Eq. (61), corresponding to either the unbalanced force or to the incremental loading, the corresponding displacements can be obtained through Eq. (38) (i.e. $\Delta\mathbf{u}=\mathbf{F}\cdot\tilde{\mathbf{v}}$). It is clear that Eq. (61) can be applied in both Total Lagrangian formulation or an Updated Lagrangian formulation, by setting the displacements $\mathbf{u}(\mathbf{X})$ of the preceding solution accordingly.

3.5 Corrector Iterations Based on the Local Weak Forms of the Noether/Eshelby Energy Conservation Laws in the Current Configuration:

Eq. (61) represents the linearized weak forms of the Noether/ Eshelby energy conservation laws based on the configurational changes in the initial configuration , to compute the predictor solution. An iteration process is necessary to correct the trial solution in configuration $C^{(N+1)}$, if it does not satisfy the solution exactly. The

third term of the residual forces in Eq. (61) has a physical meaning as the rate of work done by the unbalanced forces of the $C^{(N)}$ trial solutions in the configuration $C^{(N)}$. It has the form, before applying the divergence theorem, as,

$$\left(\delta e_{(N)}^{(N+1)}\right)^{residual\,(I)} = \int_{\Omega_N^{(I)}} \left(\sigma_{ij,i}^{(N)} + \rho_N f_j^{(N)}\right) \delta x_j d\Omega \tag{64}$$

This term is used essentially to enforce the Newtonian momentum balance laws in terms of the Cauchy stress in the deformed configuration. It implies that the present MLPG-Eshelby method enforces both the momentum balance laws through the predictor iteration process, as well as the energy conservation laws through the corrector iteration process. The MLPG-Eshelby method -based predictor allows for the discontinuity within the trial function, as shown in above.

On other hand, the predictor, along with its iterations, is based on the known configuration, and may not be valid if "defects" are developed in the solid during the current increment of deformation. Thus, corrector iterations may also be performed based on the path-independent integrals for the Eulerean Eshelby stress tensor in the current configuration, namely the stress tensor $\tilde{\mathbf{S}}$. With Eq. (18), one may compute $\tilde{\mathbf{S}}$ in the configuration $C^{(N+1)}$ as,

$$\tilde{\mathbf{S}}^{(N+1)} = \tilde{W}^{(N+1)}\,\mathbf{I} - \boldsymbol{\sigma}^{(N+1)} \tag{65}$$

The corresponding corrector iterations are performed, based on the local weak forms of the Noether/Eshelby energy conservation laws in the current configuration $C^{(N+1)}$ shown in Fig. 5, with the use of Eq. (30)c, as,

$$\begin{aligned}\left(\delta e_{(0)}^{(N+1)}\right) &= \int_\Omega [JF_{Ik}^{-1}\tilde{S}_{kl}^{(N+1)}F_{lJ}]_{,I}\delta X_J d\Omega - \int_\Omega \rho_0 b_J \delta X_J d\Omega \\ &= \int_{\partial\Omega_{N+1}} n_i \tilde{S}_{ij}^{(N+1)}\delta x_j dS - \int_{\Omega_{N+1}} \tilde{S}_{ij}^{(N+1)}\delta x_{j,i} d\Omega - \int_{\Omega_{N+1}} \rho\, b_j \delta x_j d\Omega = 0 \quad \text{for} \quad \forall\Omega_{N+1}\end{aligned} \tag{66}a$$

One may choose constant test functions $\delta\mathbf{x}$ over the subdomain and re-write Eq. (66)a as,

$$\left(\delta e_{(0)}^{(N+1)}\right) = \int_{\partial\Omega_{N+1}} n_i(\tilde{W}^{(N+1)}\delta_{ij} - \sigma_{ij}^{(N+1)})\delta x_j dS - \int_{\Omega_{N+1}} \rho\, b_j \delta x_j d\Omega = 0 \ \text{ for } \ \forall\Omega_{N+1} \tag{66}b$$

which is in general the weak form of the Noether/Eshelby energy conservation law in the current configuration [Han and Atluri (2014)].

It thus follows that both the Newtonian momentum balance laws as well as the Noether/ Eshelby the energy conservation laws need to be satisfied to ensure that the trial functions are the true solutions. In the present MLPG-Eshelby Methods, the Newtonian momentum balance laws are enforced directly through the iteration process, regardless of the continuity of the trial function. For elastic materials, it can be verified that Eq. (66) is always satisfied within in each local sub-domain if the trial function is so chosen that the strong form of the momentum equilibrium is satisfied, which implies that no energy is lost within a local sub-domain. Thus, the energy conservation laws are enforced across the inter-subdomain boundaries and lead to the predictor in Eq. (61) which ensures that the inter-subdomain boundary remains "unruptured" during finite deformation. On other hand, one may predefine

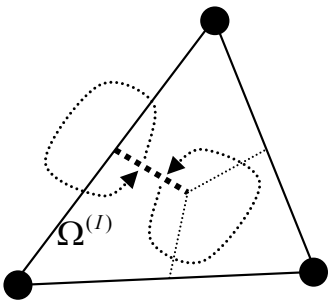

Figure 7: A closed path across the inter-sub-domain boundary.

an enclosed path, as shown in Fig. 7, and track the energy portion of the weak form in Eq. (66)b, as

$$\int_{\partial\Omega_{N+1}} \tilde{W}^{(N+1)} n_i \delta x_i dS \tag{67}$$

while the stress portion may be evaluated based on the Cauchy Stress in the deformed configuration. By assuming the possible development of defects or rupture between two local subdomains, the forces on the defects can be computed through Eq. (66) during the iteration process. If the development of a crack is assumed, the corresponding integral becomes the criterion to initiate and control the damage development processes, especially the crack development [Nikishkov and Atluri (1987), Nishioka and Atluri (1983,1989), Han and Atluri (2003)]. This will be explored in detail in our forthcoming papers for the development of ruptures in the solid during finite deformations.

3.6 Galerkin FEM vs the MLPG Eshelby methods

	The Galerkin FEM	The MLPG Eshelby Methods
Basic principle	The Newtonian momentum balance laws	The Noether/Eshelby energy conservation laws
The strong form	The Cauchy stress tensor in the current configuration: $\sigma_{ij,i}+\rho f_j=0$	The Eshelby stress tensor in the initial configuration: $T_{IJ,I}=\rho_0 b_J$
The transformed two-leg tensor form	The first Piola-Kirchhoff stess tensor of the forward deformation: $P_{Ij,I}+\rho_0 f_j=0$	The first Piola-Kirchhoff stress tensor of the inverse deformation: $\tilde{P}_{iJ,i}-\rho\, b_J=0$
The alternate strong form based on the "weighted" transformed form	The "weighted" first Piola-Kirchhoff stress tensor of the inverse deformation $\left(\tilde{P}_{iK,i}-\rho\, b_K\right)F^{-1}_{Kj}=0$	The "weighted" first Piola-Kirchhoff stress tensor of the forward deformation $\left(P_{Ik,I}+\rho_0 f_k\right)F_{kJ}=0$
Trial functions	Forward displacements $u_i(X_I)=x_i-X_I$	Configurational changes of the initial configuration, and the induced displacement: $\tilde{v}_I(X_I)$
Test functions	Variation of displacement $\delta u_i(X_I)$	Configurational changes of the deformed configuration $\delta x_i=F_{iJ}\delta X_J$
Weakform for Piecewise Linear Predictor Solutions	Global weakforms $\int_\Omega (S_{IM}F_{j,M})_{,I}\delta u_{j,L}d\Omega$ $+\int_\Omega \rho_0 f_j \delta u_{j,K}d\Omega=0$	Local weakforms over subdomains $\int_V T_{IJ,I}\delta X_J d\Omega$ $=\int_V \rho_0 b_J \delta X_J d\Omega$

	The Galerkin FEM	The MLPG Eshelby Methods
Corrector Iteration	The momentum balance laws of the Cauchy stess tensor in the current configuration $\sigma_{ij,i} + \rho f_j = 0$	The momentum balance laws of the Cauchy stress tensor in the current configuration: $\sigma_{ij,i} + \rho f_j = 0$ Weighted path-independent integrals of the energy conservation laws of the Eshelby stress tensor in the current configuration: $[JF_{Ik}^{-1}\tilde{S}_{kl}F_{lJ}]_{,I} - \rho_0 b_J = 0$
Type of Method	Mostly Galerkin FEM, leading to symmetric and sparse tangent stiffness matrics	Necessarily Petrov-Galerkin Approaches MLPG-Eshelby Approaches lead to unsymmetric and sparse tangent stiffness matrices
Continuity requirement	u_i : C_0 continuity δu_i : C_0 continuity	$\tilde{v}_I$: piece-wise continuous; discontinuous at local subdomain-boundaries δx_i: piece-wise continuity; discontinuous at local subdomain-boundaries

3.7 Some remarks On the MLPG Eshelby Methods

i) No continuity requirement across local subdomains, for the trial functions. The trial functions within a local sub-domain can be so constructed as to satisfy the geometric identities in Eqs. (29) and (32), [i.e. $(JX_{I,k})_{,I} = 0$ and $(jx_{i,K})_{,i} = 0$] exactly. This improves the numerical solution, its accuracy and its rate of convergence.

ii) Because no inter-subdomain continuity is required, discontinuities may be naturally introduced based on the energy conservation criteria. In the present MLPG Eshelby approach, surface-type discontinuities may also be introduced between local sub-domains, to form explicit cracks.

iii) Iteration based on the energy conservation laws provides additional corrections to other non-elastic processes and if multi-physics are also involved.

The key for the use of the weakforms of the Noether/ Eshelby energy conservation laws is to construct the invertible mapping relationships between the variables in all configurations, which also need to be compatible to satisfy the geometric identities in Eqs. (29) and (32). It is not possible to define such a mapping relation between the configurations in a global domain. In contrast, the local linearized invertible and compatible relations between the configurations may be easily achieved by constructing a proper local deformation field with the use of invertible closed form functions. The invertible and compatible relationships can be defined in terms of the constant coefficients of the closed form functions, and thus leads to local meshless methods, and the MLPG method of Atluri (1998,2004), in a very natural way.

The trial functions $\tilde{\mathbf{v}}$ are the configurational changes of the initial configuration. In the present study, the trial functions $\tilde{\mathbf{v}}$ are employed in the weakforms directly, instead of the resulting displacements in the deformed configuration [i.e. the displacements $\Delta\mathbf{u}$]. The trial functions $\tilde{\mathbf{v}}$ need to be admissible movements within the local neighboring domains because the resulting displacements (i.e. $\Delta\mathbf{u} = \mathbf{F}\cdot\tilde{\mathbf{v}}$) need to satisfy the boundary conditions. The test functions $\delta\mathbf{x}$ have a physical meaning of configurational changes in the current configuration. It is convenient to choose the test functions $\delta\mathbf{x}$ to be linear within each test domain, such as rigid body motion and rotation or simple uniform deformations which have been used in writing the weakforms of the energy conservation laws in Section 3 of our previous paper [Han and Atluri (2014)]. It is clear that the test functions need to be kept completely independent from the trial functions . Hence, it becomes very natural that the (Meshless Local Petrov-Galerkin) MLPG Eshelby approach is essential for developing numerical methods for preserving the energy conservation laws, by properly choosing trial and test functions over non-overlapping sub-domains.

3.8 Numerical implementation

In the present study, the first MLPG-Eshelby method is formulated by choosing $\tilde{\mathbf{v}}^{MLS}$ as the trial functions, and $\delta\mathbf{x}^{FEM}$ as the test functions. We call this the "Primal MLPG-Eshelby Method". The domain integrals in Eq. (61)a are performed over the local subdomain domain without any discontinuities.

The second MLPG-Eshelby method is formulated by choosing $\tilde{\mathbf{v}}^{MIX}$ as the trial functions and $\delta\mathbf{x}^{FVM}$ as the test functions, and labeled as the "Mixed MLPG Eshelby method". Only boundary integrals in Eq. (61)c are performed over the boundaries between local sub-domains.

The third MLPG-Eshelby method is formulated by choosing $\boldsymbol{\sigma}^{MIX}$ as the trial functions and $\delta\mathbf{x}^{FEM}$ as the test functions, and labeled as the "Mixed Stress MLPG Eshelby method". The domain integrals in Eq. (61)a are performed over the solution domain without any discontinuities. This method becomes very simple as the do-

main integral needs to be computed once for the system stiffness matrix as well as residual forces.

4 Linear Elasto-Static Analysis

For a linear elastic body undergoing infinitesimal deformations, the system equations may be formed, using the piecewise linear predictor methodology presented in the previous Section, by setting the preceding solution $\mathbf{u}(\mathbf{X})$ be zero and $\mathbf{F}(\mathbf{X})$ to be an identity matrix.

4.1 Patch test

The first example is that of a standard patch test. The material parameters are taken as Young's Modulus $E = 1.0$, and Poisson Ratio $\nu = 0.25$. Two nodal configurations are used, a regular one and an irregular one, as shown in Fig. 8.

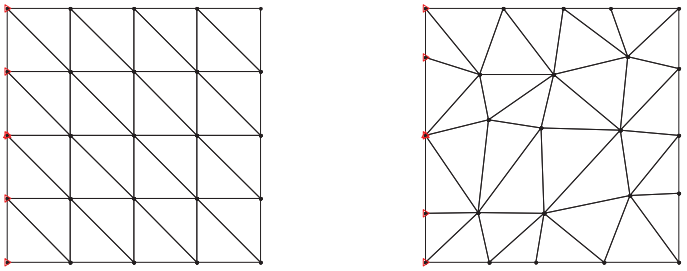

(a) regular configuration (b) irregular configuration

Figure 8: Nodal configuration for patch test.

4.2 A problem with a Quadratic Solution: a Higher-Order Patch Test

A second order analytical solution is used for patch test with the same nodal configurations in Fig. 9, as

$$\mathbf{u} = \{x^2 - y^2, -2xy\} \tag{68}$$

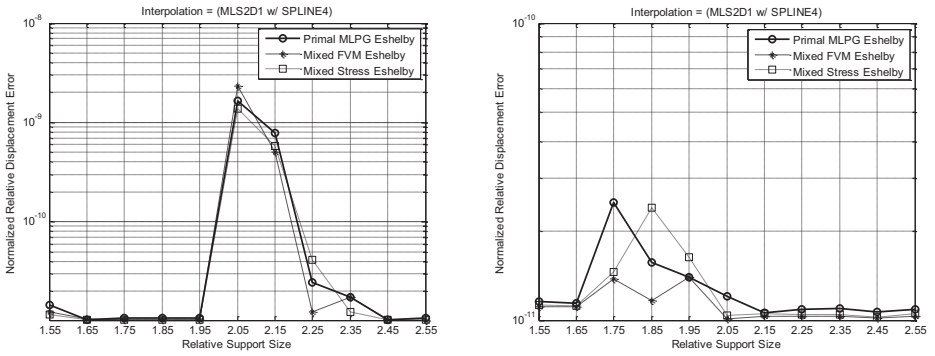

(a) regular configuration (b) irregular configuration

Figure 9: Normalized displacement error of a patch under uniform tension.

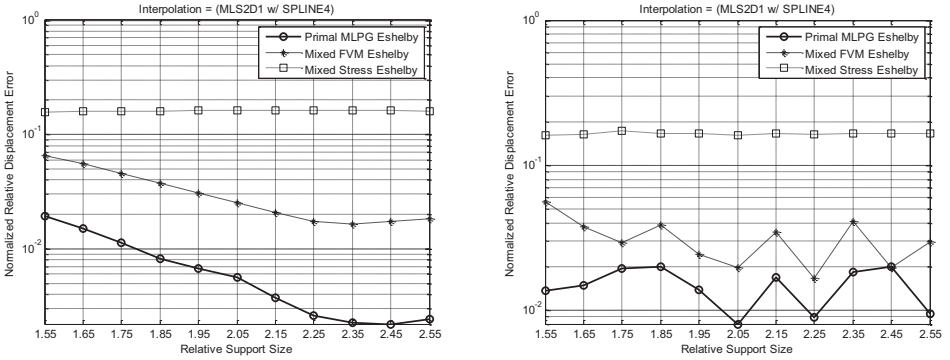

(a) regular configuration (b) irregular configuration

Figure 10: Normalized displacement error of a patch under second order nonlinear deformation.

4.3 Cantilever beam

A cantilever beam under a transverse load, as shown in Fig. 11, for which the following exact solution is given in Timoshenko and Goodier (1970):

$$
\begin{aligned}
u_x &= -\frac{Py}{6\bar{E}I}\left[3x(2L-x)+(2+\bar{\upsilon})(y^2-c^2)\right] \\
u_y &= \frac{P}{6\bar{E}I}\left[x^2(3L-x)+3\bar{\upsilon}(L-x)y^2+(4+5\bar{\upsilon})c^2x\right]
\end{aligned}
\tag{69}
$$

where the moment of inertia I the beam is given as,

$$I = \frac{c^3}{3} \tag{70}$$

Two nodal configurations are created with 39 nodes and 125 nodes in Fig. 12 and Fig. 15, respectively. The irregular configurations are also created by introducing 30% random variation from the regular configurations. The numerical results show that the present MLPG Eshelby methods are very stable and mesh insensitive. A convergence study is also performed as shown in 5.

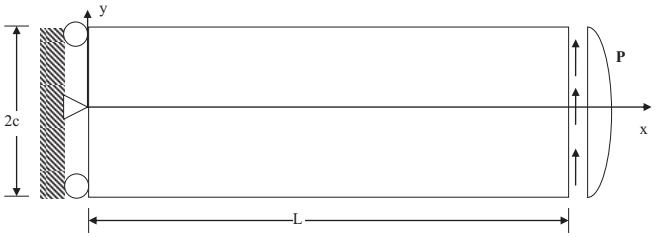

Figure 11: A cantilever beam under an end load (L=24, c=2).

(a) regular configuration (b) irregular configuration

Figure 12: Nodal configuration for a cantilever beam (39 nodes).

5 Finite Deformation Nonlinear Analysis

For a hyperelastic body undergoing finite deformations, the Total Lagrangian formulation is implemented for the Mixed MLPG Eshelby method in Eq. (61)c. The outline of the complete solution algorithm is shown in Box 1, in which the system matrix is updated only once during every load increment, instead of every iteration. It may be changed to the Updated Lagrangian formulation by revising the displacement updating and deformation gradient computing processes accordingly, as no stress update process is necessary.

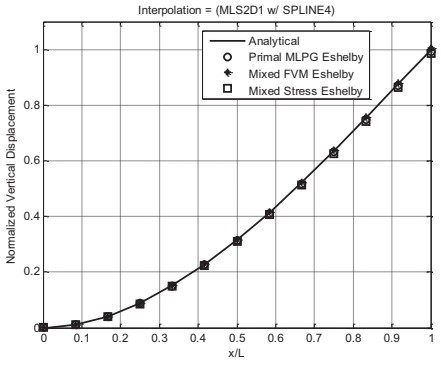

(a) regular configuration

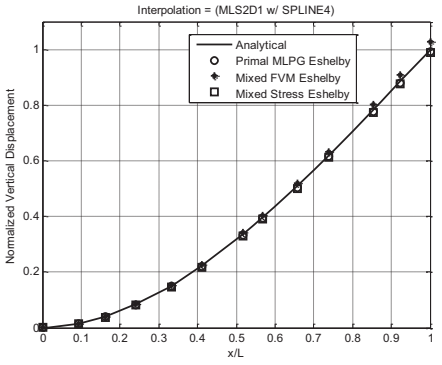

(b) irregular configuration

Figure 13: Normalized vertical displacement of a cantilever beam under an end loading (39 nodes).

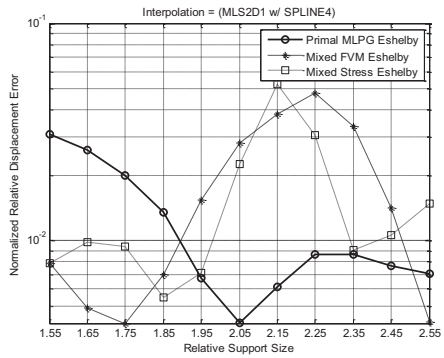

(a) regular configuration

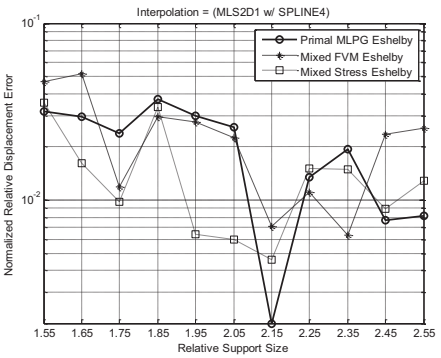

(b) irregular configuration

Figure 14: Normalized displacement error of a cantilever beam under an end loading (39 nodes).

(a) regular configuration (b) irregular configuration

Figure 15: Nodal configuration for a cantilever beam (125 nodes).

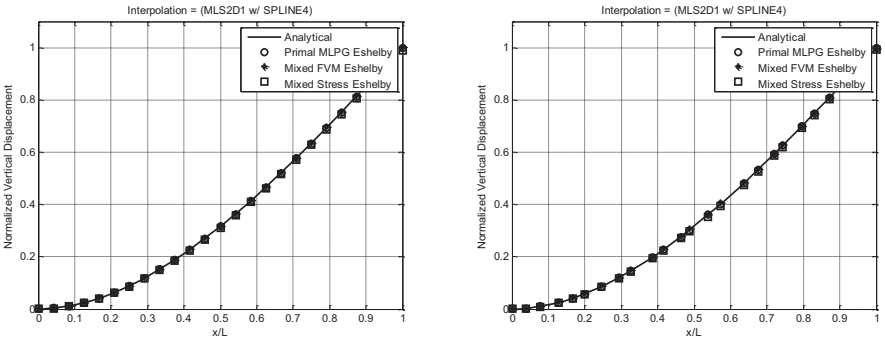

(a) regular configuration (b) irregular configuration

Figure 16: Normalized vertical displacement of a cantilever beam under an end loading (125 nodes).

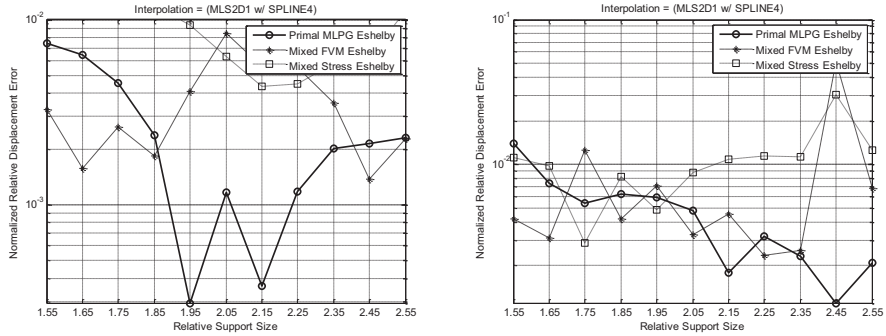

(a) regular configuration (b) irregular configuration

Figure 17: Normalized displacement error of a cantilever beam under an end loading (125 nodes).

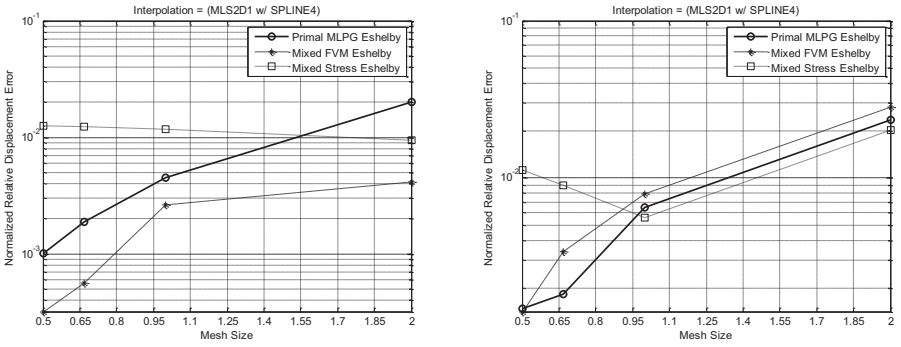

(a) regular configurations (b) irregular configurations

Figure 18: Convergence rate in a cantilever beam under an end load (with 39 nodes, 125 nodes, 259 nodes, and 441 nodes respectively).

A generalized Neo-Hookean material model is adopted in the present paper with a strain energy density function as given in [Bower (2009)],

$$W = \frac{G}{2}(\bar{I}_1 - 3) + \frac{K}{2}(J-1)^2 \tag{71}$$

where G and K are the shear modulus and bulk modulus; $\bar{I}_1$ is the first invariant of the deviatoric part of the left Cauchy-Green deformation tensor $\mathbf{B}$; $J = \det(\mathbf{F})$ is the determine of the deformation gradient. The Cauchy stress is given as

$$\sigma_{ij} = \frac{G}{J^{5/3}}(B_{ij} - \frac{B_{qq}}{3}\delta_{ij}) + K(J-1)\delta_{ij} \tag{72}$$

and the tangential material stiffness,

$$\begin{aligned} c_{ijkl} = & \frac{G}{J^{2/3}}[\frac{1}{2}(\delta_{ik}B_{jl} + \delta_{jl}B_{ik} + B_{il}\delta_{jk} + B_{jk}\delta_{il}) - \frac{2}{3}(B_{ij}\delta_{kl} + B_{kl}\delta_{ij}) \\ & + \frac{2}{3}\frac{B_{qq}}{3}\delta_{ij}\delta_{kl}] + K(2J-1)J\delta_{ij}\delta_{kl} \end{aligned} \tag{73}$$

In the present paper, the normalized shear modulus $G = 1$ and the bulk modulus $K = 10$. The corresponding Poisson ratio is $\nu = 0.4516$. The system matrix is updated once every load increment with the tangential stiffness matrix defined in Eq. (80) in Appendix A.

Box 1: T.L. formulation of the MLPG Mixed Eshelby method

- INPUT model Information
- RUN Delaunay algorithm to create local subdomains
- INITIALIZE load $\mathbf{f}_{[0]}$, displacements $\mathbf{u}_{[0]}$, and the unbalanced force $\mathbf{r}_{[0]}^{[0]}$
- LOOP over load increments n
  - ASSEMBLE the system matrix $\mathbf{K}_{[n]}^{tangent}$ over boundaries of all local sub-domains (l.h.s. of Eq. (61)c), with the tangent material stiffness in Eq. (59).
  - FIND load increment $\Delta\mathbf{f}_{[n]}$
  - SET $\mathbf{f}_{[n]} = \mathbf{f}_{[n-1]} + \Delta\mathbf{f}_{[n]}$
  - SET $\mathbf{r}_{[n]}^{[0]} = \mathbf{r}_{[n-1]}^{[last]} + \Delta\mathbf{f}_{[n]}$
  - DO iteration i
    - SOLVE system equations $\mathbf{K}_{[n]}^{tangent}\ \tilde{\mathbf{v}}_{[n]}^{[i]} = \mathbf{r}_{[n]}^{[i-1]}$
    - COMPUTE displacement increment $\Delta\mathbf{u}_{[n]}^{[i]} = \mathbf{F}_{[n]}^{[i-1]} \cdot \tilde{\mathbf{v}}_{[n]}^{[i]}$
    - UPDATE displacements $\mathbf{u}_{[n]}^{[i]} = \mathbf{u}_{[n]}^{[i-1]} + \Delta\mathbf{u}_{[n]}^{[i]}$
    - COMPUTE nodal deformation gradients $\mathbf{F}_{[n]}^{[i]}$
    - COMPUTE nodal stresses $\boldsymbol{\sigma}_{[n]}^{[i]}$
    - ASSEMBLE the residual force $\mathbf{r}_{[n]}^{[i]}$ over boundaries of all local sub-domains (r.h.s. of Eq. (61)c)
    - COMPUTE the error as a function of $\left\{\left\|\mathbf{r}_{[n]}^{[i]}\right\|, \left\|\mathbf{f}_{[n]}\right\|, \left\|\Delta\mathbf{u}_{[n]}^{[i]}\right\|, \left\|\mathbf{u}_{[n]}^{[i]}\right\|\right\}$
  - WHILE ($error > tolerence$)
- ENDLOOP

5.1 Patch test

The first example is that of a standard patch test. Two nodal configurations are used, a regular one and an irregular one, as shown in Fig. 19 (same as Fig. 8). The uniform tension is applied on one side. The total nominal stress of 3 is applied in 10 uniform increments. The numerical results in Fig. 20 and Fig. 21 show that the Mixed MLPG Eshelby method passes the patch test.

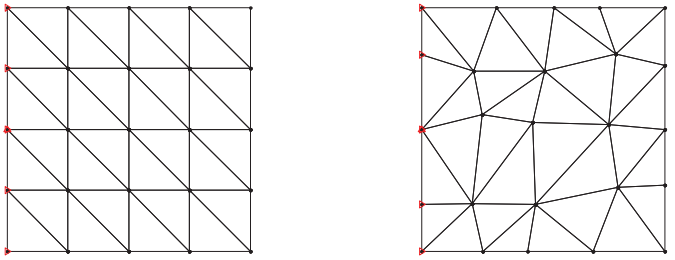

(a) regular configuration (b) irregular configuration

Figure 19: Nodal configuration for hyperelastic patch test.

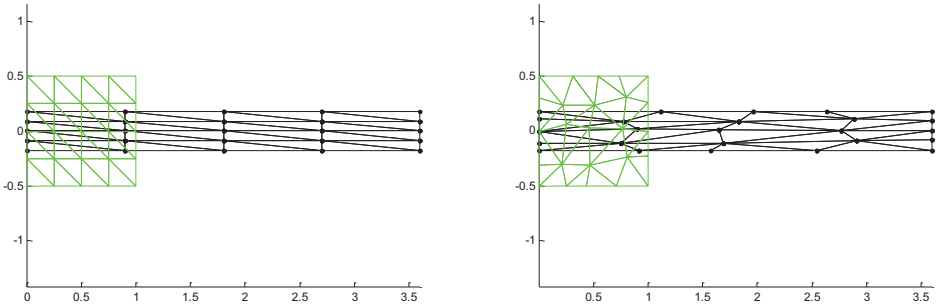

(a) regular configuration (b) irregular configuration

Figure 20: Final deformed configuration of hyperelastic patch test.

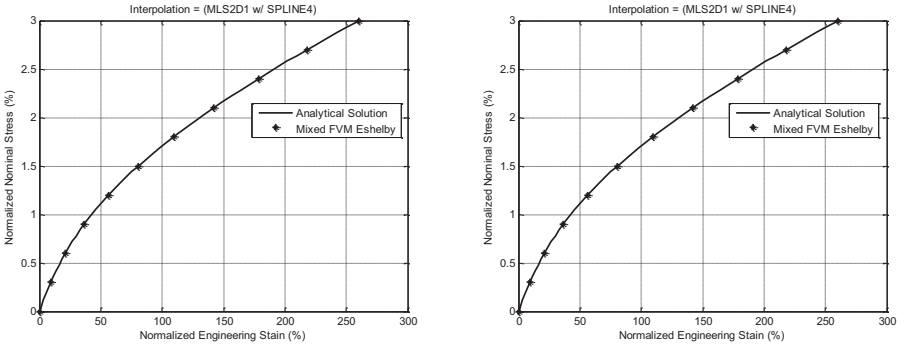

(a) regular configuration (b) irregular configuration

Figure 21: Load-displacement curve of hyperelastic patch test.

5.2 Finite-strain analysis of a hyperelastic plate

A patch under a tension load with one fixed end, as shown in Fig. 22, is modeled. The symmetric boundary condition is applied along the X-axis. Two nodal configurations are also used, a regular one and an irregular one, as shown in Fig. 19. The final deformed configurations are shown in Fig. 23, and the load-displacement curves are shown in Fig. 24. It shows that the present Mixed MLPG Eshelby method is not sensitive to the irregularity of the configurations.

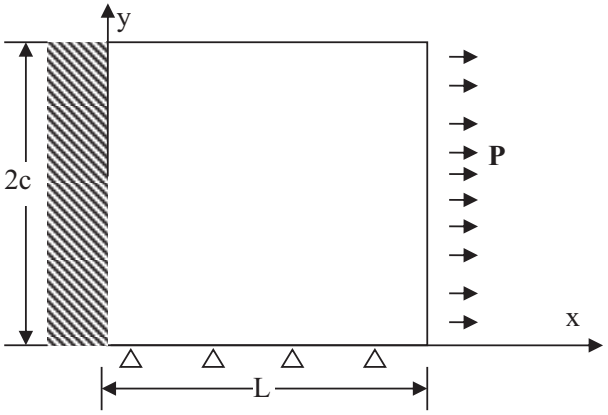

Figure 22: A clamped patch under tension (L=1, c=0.5).

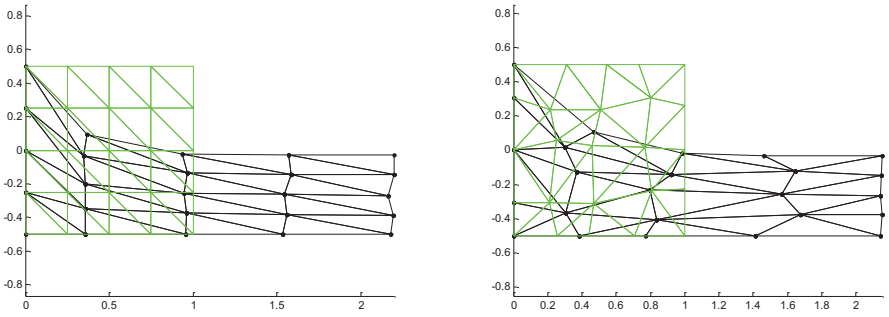

(a) regular configuration (b) irregular configuration

Figure 23: Final deformed configuration of a clamped hyperelastic patch.

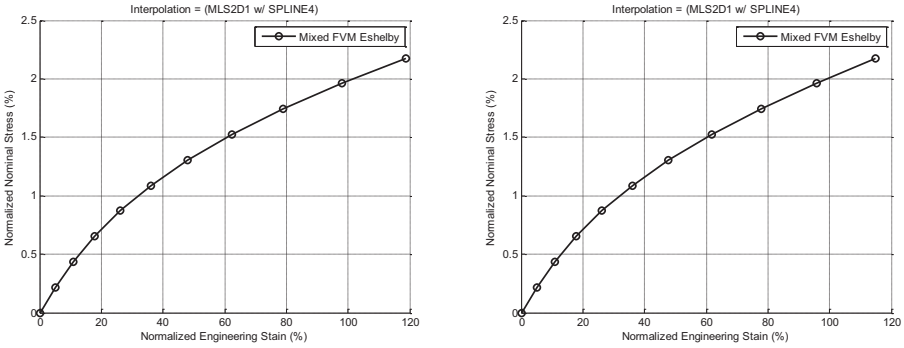

(a) regular configuration (b) irregular configuration

Figure 24: Load-displacement curve of a clamped hyperelastic patch.

6 Conclusions

In the present MLPG-Eshelby approach, the use of local (and possibly discontinuous) meshless trial and test functions $\delta\mathbf{X}$ (configurational changes in the initial configuration) and $\delta\mathbf{x}$ (configurational changes in the current configuration) , respectively, which satisfy the geometric identities of Eqs. (29) and (32) possibly identically in a local fashion, is radically different from the presently popular FEM approach for finite deformation (large strain and large rotations) solid mechanics. From the numerical solutions presented for hyperelastic solids, it is found that the present MLPG-Eshelby Method which produces both piecewise linear predictor as well as corrector solutions, based on the local weak-forms of the Noether/Eshelby conservation laws in the deformed and undeformed configurations, respectively, converges much faster and produces much better accuracies, than the currently popular FEM. While finite deformations of hyperelastic solids are only considered in the present paper, plasticity and dynamic deformation will be considered in our forthcoming papers.

Acknowledgement: The work of the second author was fruitfully concluded while he spent a very brief period of time, in January 2014, at the Texas Institute for Advanced Study at Texas A&M University. The support of TIAS, and the many discussions with its Director, John L. Junkins, are thankfully acknowledged.

References

Atluri, S. N. (1975): On 'Hybrid' Finite Element Models in Solid Mechanics. *Advances in Computer Methods for Partial Differential Equations, R. Vichrevetsky, Ed.*, AICA, pp. 346-355.

Atluri, S. N. (1980): On Some New General and Complementary Energy Theorems for the Rate Problems in Finite Strain, Classical Elastoplasticity. *Journal of Structural Mechanics*, vol. 8, no. 1, pp. 61-92.

Atluri, S. N. (1982): Path-Independent Integrals in Finite Elasticity and Inelasticity with Body Forces, Inertia, and Arbitrary Crack-Face Conditions. *Engineering Fracture Mechanics*, vol. 16, no. 3, pp. 341-364.

Atluri, S. N. (1984a): Alternate stress and conjugate strain measures, and mixed variational formulations involving rigid rotations, for computational analyses of finitely deformed solids, with application to plates and shells—I: Theory. *Computers and Structures*, vol. 18, no. 1, pp. 93–116.

Atluri, S. N. (1984b): On Constitutive Relations at Finite Strain: Hypo-Elasticity and Elasto-Plasticity with Isotropic or Kinematic Hardening. *Computer Methods in Applied Mechanics and Engineering*, vol. 43, no. 2, pp. 137-171.

Atluri, S. N. (2004): *The Meshless Local Petrov-Galerkin (MLPG) Method for Domain & Boundary Discretizations.* Tech Science Press, 665 pages.

Atluri, S. N.; Cazzani, A. (1995): Rotations in Computational Solid Mechanics, Invited Feature Article. *Archives for Computational Methods in Engg., ICNME, Barcelona, Spain*, vol. 2, no. 1, pp. 49-138.

Atluri, S. N.; Han, Z. D.; Rajendran, A. M. (2004): A New Implementation of the Meshless Finite Volume Method, Through the MLPG "Mixed" Approach. CMES: *Computer Modeling in Engineering & Sciences*, vol. 6, no. 6, pp. 491-514.

Atluri, S. N.; Zhu, T. (1998): A new meshless local Petrov-Galerkin (MLPG) approach in computational mechanics. *Comput. Mech.*, vol. 22, pp.117-127.

Bower, A. F. (2009): *Applied Mechanics of Solids*, http://solidmechanics.org.

Eshelby, J. D. (1951): The Force on an Elastic Singularity. *Phil. Trans. R. Soc. Lond. A*, vol. 244, pp. 87-112.

Eshelby, J. D. (1975): The elastic energy-momentum tensor. *Journal of Elasticity*, vol. 5, nos. 3-4, pp. 321-335.

Han, Z. D.; Atluri, S. N. (2003): On simple formulations of weakly-singular tBIE&dBIE, and Petrov-Galerkin approaches. *CMES: Computer Modeling in Engineering & Sciences*, vol. 4, no. 1, pp. 5-20.

Han, Z. D.; Atluri, S. N. (2014): Eshelby Stress Tensor **T**: a Variety of Conservation Laws for **T** in Finite Deformation Anisotropic Hyperelastic Solid & Defect Mechanics, and the MLPG-Eshelby Method in Computational Finite Deformation Solid Mechanics-Part I. *CMES: Computer Modeling in Engineering & Sciences*, vol. 97, no. 1, pp. 1-34.

Nishioka, T.; Atluri, S. N. (1983): Path-Independent Integrals, Energy Release Rates, and General Solutions of Near-Tip Fields in Mixed-Mode Dynamic Fracture Mechanics. *Engineering Fracture Mechanics*, vol. 18, no. 1, pp. 1-22.

Nikishkov, G. P.; Atluri, S. N. (1987): Calculation of Fracture Mechanics Parameters for an Arbitrary 3-D Crack by the EDI Method. *International Journal for Numerical Methods and Engineering*, vol. 24, pp. 1801-1822.

Nishioka, T.; Atluri, S. N. (1989): On the Path Independent Integral T* in Nonlinear and Dynamic Fracture Mechanics. *Nuclear Engineering and Design*, vol. 111, pp. 109-121.

Noether, E. (1918): Invariante Variationsprobleme, *Göttinger Nachrichten, Mathematisch-physikalische Klasse*, vol. 2, p. 235. (English translation by M. A. Tavel, Transport Theory and Statistical Physics, vol. 1, p. 183, 1971).

Rubinstein, R.; Atluri, S. N (1983): Objectivity of Incremental Constitutive Relations Over Finite Time Steps in Computational Finite Deformation Analysis. *Computer Methods in Applied Mechanics & Engineering*, vol. 36, pp. 277-290.

Appendix A: The rate-based tangential stiffness matrices

A.1 Linerarization

Let $\mathbf{w}(\mathbf{x})$ be the velocity of a material particle in the current configuration, $C^{(N)}$, and let the velocity gradient, denoted here as $\mathbf{L}$, be

$$\mathbf{L} = \frac{\partial \mathbf{w}}{\partial \mathbf{x}} = \mathbf{D} + \mathbf{W} \quad \text{or} \quad L_{ij} = \frac{\partial w_i}{\partial x_j} = D_{ij} + W_{ij} \tag{74}$$

where $\mathbf{D}$ is the strain rate and $\mathbf{W}$ is the spin rate, as

$$\mathbf{D} = \frac{1}{2}(\mathbf{L} + \mathbf{L}^t); \quad \mathbf{W} = \frac{1}{2}(\mathbf{L} - \mathbf{L}^t) \tag{75}$$

Let $\dot{\boldsymbol{\sigma}}^*$ is the Jaumann rate of the Kirchhoff stress $\boldsymbol{\sigma}^* = (J\boldsymbol{\sigma})$, which is given through a rate potential [Atluri (1980)], as

$$\dot{\boldsymbol{\sigma}}^* = \mathbf{c}^* : \mathbf{D} \tag{76}$$

where $\mathbf{c}$ is the tangent material stiffness tensor of 4^{th} order.

The corresponding rate of the second Piola-Kirchhoff stress tensor is given as [Atluri (1980); Rubinstein and Atluri (1983); Atluri and Cazzani (1995)]:

$$\dot{\mathbf{S}} = \frac{d\mathbf{S}}{dt} = \dot{\boldsymbol{\sigma}}^* - \mathbf{D}\cdot\boldsymbol{\sigma} - \boldsymbol{\sigma}\cdot\mathbf{D} \tag{77}$$

Thus the tangential material stiffness for the energy conversation laws in Eq. (59) can be written in the rate form, with Eqs. (76)&(77), as,

$$\dot{\mathbf{S}} + \boldsymbol{\sigma}\cdot\mathbf{L}^t = \dot{\boldsymbol{\sigma}}^* - \mathbf{D}\cdot\boldsymbol{\sigma} - \boldsymbol{\sigma}\cdot\mathbf{W} = \mathbf{c}^* : \mathbf{D} - \mathbf{D}\cdot\boldsymbol{\sigma} - \boldsymbol{\sigma}\cdot\mathbf{W} \equiv \mathbf{c}^{tangent} : \mathbf{L}^t \tag{78}$$

or in the incremental form, Eq. (59) can be re-written as,

$$\left(\Delta S^{(N+1)}_{(N)}\right)_{IJ} + \sigma^{(N)}_{IM}\left(\Delta F^{(N+1)}_{(N)}\right)_{jM} = c^{tangent}_{ijkl}\Delta L_{lk} \tag{79}$$

If $c^{tangent}_{ijkl}$ is linearized in $C^{(0)}$ with respect to ΔL_{lk}, the third and forth indices needs to be pulled back with $\mathbf{F}$ and $\mathbf{F}^{-1}$, respectively, as

$$c^{tangent}_{ijkl} F_{kM} F^{-1}_{Nl} \Delta L_{nm} = c^{tangent}_{ijkl} \Delta L^*_{KL} \tag{80}$$

in which Eq. (39)b is used. With the consideration of Eq. (19), it means that $\Delta\mathbf{L}^t_{(N)}$ may be replaced by $\Delta\mathbf{L}^*_{(0)}$ for better prediction if the system equations are linearized in the configuration $C^{(0)}$, rather than pulling-back the tangential material stiffness matrix explicitly.

A.2 Numerical study

In the present paper, Eq. (80) is implemented for the hyperelastic material. The convergence rate of the patch test example is compared between the present Mixed MLPG Eshelby method and the classic FEM method [Bower (2009)] with a coarse mesh as shown in Fig. 25. The numbers of iterations during each load increment are listed in Table. 1. The displacement increments during iterations of the first and second load increments are charted in Table. 2 and Table. 3, respectively. It shows that the present MLPG method gives a better convergence rate. The diagonal element of the system equation corresponding to the center node in Fig. 25 are listed in Table. 4. The tangent material stiffness components $c^{tangent}_{1111}$ and $c^{tangent}_{2222}$ of the present MLPG method are also listed in Table. 4. It confirms that the present Mixed MLPG Eshelby method possesses a numerically stable tangent stiffness matrix.

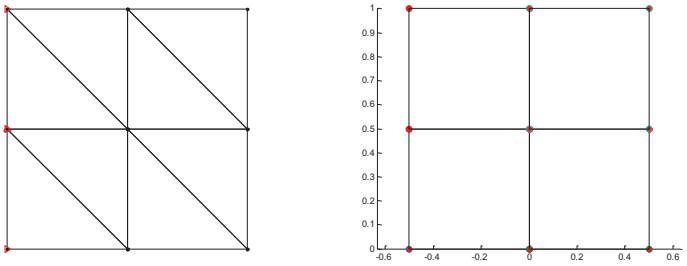

(a) Mixed MLPG Eshelby method (b) Finite Element

Figure 25: Nodal configuration for hyperelastic patch test.

Table 1: Number of Iterations

Load Step	1	2	3	4	5	6	7	8	9	10
FEM	8	8	11	17	28	35	29	20	15	11
MLPG	5	7	7	7	8	8	8	8	8	9

Table 2: Displacement during the first load increment

Iteration #	FEM		MLPG	
	Displacement	Error	Displacement	Error
1	0.082258	1.000000	0.089560	0.068840
2	0.089005	0.068283	0.092553	0.032221
3	0.092019	0.033329	0.092752	0.002030
4	0.092490	0.004589	0.092794	0.000465
5	0.092738	0.002763	0.092798	0.000038
6	0.092773	0.000337		
7	0.092794	0.000239		
8	0.092796	0.000025		

Table 3: Displacement during the second load increment

Iteration #	FEM		MLPG	
	Displacement	Error	Displacement	Error
1	0.197307	0.526424	0.195741	0.343258
2	0.205078	0.034832	0.205637	0.042298
3	0.210436	0.025966	0.211138	0.025414
4	0.210930	0.002529	0.211554	0.001870
5	0.211573	0.003202	0.211657	0.000483
6	0.211580	0.000321	0.211667	0.000045
7	0.211665	0.000437	0.211669	0.000008
8	0.211658	0.000071		

Table 4: The tangent material stiffness for each load increment

Load Step	Engng. Strain (%)	FEM		MLPG		MLPG	
		K_{xx}	K_{yy}	K_{xx}	K_{yy}	$c_{1111}^{tangent}$	$c_{2222}^{tangent}$
1	0.00	16.4444	16.4444	6.7524	6.7524	11.3333	11.3333
2	9.28	14.2647	19.4004	6.6043	7.5200	11.5940	11.7033
3	21.17	12.1236	23.6373	6.5089	8.5635	11.9115	12.1539
4	36.51	10.0976	29.8827	6.5385	10.0086	12.3114	12.7210
5	56.12	8.2874	39.1899	6.8167	12.0203	12.8266	13.4511
6	80.42	6.7775	52.8928	7.5209	14.7865	13.4917	14.3938
7	109.26	5.5931	72.4779	8.8626	18.4978	14.3345	15.5901
8	142.11	4.7006	99.4509	11.0678	23.3495	15.3732	17.0680
9	178.46	4.0356	135.4098	14.3771	29.5630	16.6190	18.8466
10	217.93	3.5348	182.1935	19.0611	37.4045	18.0809	20.9423